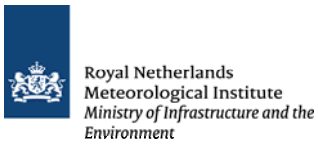

Ocean and Sea Ice SAF

Scientific Report

SAF/OSI/CDOP2/KNMI/SCI/RP/213

ASCAT Quality Control near Rain

Marcos Portabella

Wenming Lin

Ad Stoffelen

Anton Verhoef

Antonio Turiel

Version 1.0

7 May 2014

DOCUMENTATION CHANGE RECORD

Reference: **SAF/OSI/CDOP2/KNMI/SCI/RP/213**

Issue / Revision :	Date :	Change :	Description :
Version 1.0	2014-05-07		Draft version

Summary

The Advanced Scatterometer (ASCAT) onboard the Metop satellite series is designed to measure the ocean surface wind vectors globally. Generally, ASCAT provides wind products at excellent quality. The quality of the Advanced Scatterometer (ASCAT) derived winds is known to be generally degraded with increasing values of the inversion residual or maximum likelihood estimator (MLE). In the current ASCAT Wind Data Processor (AWDP), an MLE-based Quality control (QC) is adopted to filter poor-quality winds, which has proven to be effective in screening artifacts in the ASCAT winds, associated with increased sub-cell wind variability, notably under rain conditions. However, some poorly verifying winds, which appear in areas with convection, are not screened by the operational QC.

Identification of rain can help to better understand the impact of geophysical effects associated with rain on scatterometer wind quality, and to develop an improved QC approach for scatterometer data processing. In the first part of this report, an image processing method, known as singularity analysis (SA), is used to detect the geophysical effects associated with rain. The performance of SA for rain detection is validated using ASCAT Level-2 data collocated with satellite radiometer rain data. The rain probability as a function of SA-derived singularity exponent (SE) parameter is calculated and compared with other rain-sensitive parameters, such as the MLE. The results indicate that the SA is effective in detecting the presence of rain in ASCAT wind vector cells (WVCs). Moreover, SA is a complementary rain indicator to the MLE parameter, thus showing great potential for an improved scatterometer QC.

In the second part of the report, SA is proposed to complement the current ASCAT QC. The implementation of this new joint QC procedure is investigated, based on a comprehensive analysis of quality-sensitive parameters using the European Centre for Medium-range Weather Forecasts (ECMWF) model winds, the Tropical Rainfall Measuring Mission's (TRMM) Microwave Imager (TMI) rain data, and tropical buoy wind and precipitation data as reference, taking into account their spatial and temporal representation. The buoy validation results show that the proposed method indeed effectively removes ASCAT winds in spatially variable conditions. It filters three times as many wind vectors as the operational QC, while preserving verification statistics with local buoys. Indeed, rain and wind variability as measured by the ASCAT SE appear well correlated. Besides rain-induced large wind variability, which is shown to degrade the quality of ASCAT-derived winds, no evidence of rain-contamination effects (e.g., rain splashing) have been found. Further analysis is required to exclude rain contamination for ASCAT.

Variable winds are a potential hazard in some applications, such as data assimilation, and the methods developed here may be useful for those applications. For other applications, such as nowcasting and oceanography it may be relevant to keep the flagged wind data since they provide essential information on (highly variable) air-sea interaction processes that cannot be spatially captured by any other wind observing system.

Contents

1 Introduction

Space-borne scatterometers are known to provide accurate mesoscale 10-m equivalent-neutral wind speed and direction. The wind field inferred from scatterometer measurements is used in a variety of applications, including Numerical Weather Prediction (NWP), nowcasting, climate and air-sea interaction modelling. The wind retrieval procedure is carried out by inverting the non-linear relationship between the averaged radar backscatter cross-sections (σ^0) and the mean sea surface wind vector in a Wind Vector Cell (WVC). However, geophysical phenomena other than WVC-mean wind, such as rain, sub-WVC wind variability, confused sea state, and land/ice contamination within the radar footprint, may also significantly contribute to the backscatter signal measured by scatterometers, and in turn, distort the mean wind-induced signal, leading to poor-quality retrieved winds. Elimination of poor-quality winds and assessing their effect is the prerequisite for using scatterometer data in the already mentioned applications.

Over the last decade, broad studies have sought to better understand the physics of poor-quality scatterometer winds. In particular, the presence of rain is known to degrade scatterometer-derived sea-surface wind quality. Rain drops both attenuate and scatter the microwave signal. Those effects are relevant for Ku-band scatterometers, but relatively small for C-band systems (except for heavy rain conditions). In addition, the splashing of rain alters the wind-induced scatterometer backscatter signature on the ocean surface. At the same time, the wind variability within a wind vector cell (WVC) is enhanced in rain scenarios, which, in turn, increases the measurement variance. If the wind retrieval does not take rain effects into account, the rain contributions are interpreted as wind features, and in turn, the retrieved wind quality is degraded. Over the last decades, several approaches have been proposed to address the mentioned rain effects on scatterometers, especially for Ku-band systems. The first approach consists of identifying the parameters that are sensitive to rain (e.g., retrieved wind speed, MLE, backscatter dependence on incidence angle, etc.), estimating the rain probability or the retrieved wind quality as a function of those parameters by using a training dataset, and then applying the probability estimation of rain or wind quality indicator to flag data as 'rain-contaminated' [1][2]. The second methodology is based on assessing the rain effects on scatterometer backscatter measurements by using collocated scatterometer wind data, satellite microwave-derived rain data, and Numerical Weather Prediction (NWP) wind data, and then correcting the rain-induced backscatter contribution before wind retrieval [3][4]. The third strategy also uses collocated scatterometer, rain and NWP wind data to model both wind- and rain-induced backscatter, with the objective of retrieving wind and rain parameters simultaneously [5][6]. Moreover, there are techniques which are based on the use of a single parameter, i.e., the Normalized Radar Cross Section (NRCS, σ^0), for rain detection purposes. For instance, the difference between horizontally polarized and vertically polarized σ^0 can be used to define the rain flag [7]. In [8], multi-fractal exponents are computed from the QuikSCAT σ^0 images, and then a threshold is set to separate the rainy cases from the rain-free cases.

For the identical C-band Advanced Scatterometers onboard Metop-A and Metop-B, i.e., ASCAT-A and ASCAT-B, a quality control (QC) based on the wind inversion residual or maximum-likelihood estimator (MLE) is developed to screen the poor-quality winds [9]. The MLE depicts the closest distance between the ASCAT measurement triplets (corresponding to the three antenna beam signals at each side of the ASCAT swath) and the geophysical model function (GMF). A large MLE

value indicates a large inconsistency of the measurement triplet with the GMF, i.e., a low probability that they can be explained by the WVC-mean wind vector. In particular, note that the current operational QC threshold is set for MLE>+18.6. The MLE is proved to be sensitive to rain, i.e., it generally increases with rain rate (RR) [10]. However, many WVCs with low MLE values (and therefore not QC-ed) are also affected by rain (i.e., the retrieved wind quality is degraded). Moreover, the MLE histogram peak of rain-contaminated WVCs is close to that of rain-free cases, which indicates that the MLE itself is ineffective in flagging rain-contaminated ASCAT WVCs in general [10]. Particularly, at low winds backscatter triplets affected by rain may still result in low or negative MLE values. At low winds, rain may cause enhanced spatial variability and techniques using spatial derivatives may be complementary in QC of rain cases.

An image-processing technique, known as singularity analysis (SA), has been recently proposed as a complementary ASCAT QC tool [10]. SA provides quantitative information about the local regularity or irregularity of the signal. It is therefore able to detect not only existing geophysical structures, characterized as singularity fronts, but also any transition due to the presence of retrieval errors. In [10], preliminary results show that SA can potentially be used for ASCAT rain identification.

In this study, the SA method is further developed for optimizing ASCAT rain identification and then further adapted and tested for QC purposes. A complementary approach using both singularity exponent (SE) and MLE is proposed to improve the current ASCAT QC. Section 2 introduces the different types of wind and rain data sources used in this study. In section 3, the singularity analysis method is briefly introduced and then applied and optimized for ASCAT data. In section 4, the experimental results of singularity analysis on rain flagging are presented and a comparison with the MLE-based rain identification is carried out. In section 5, two different QC procedures based on the combination of several quality-sensitive parameters, i.e., MLE, the measurement variability factor K_p, and the singularity exponent (SA output), are proposed and validated using collocated ASCAT data and buoy winds, taking account of the enhanced local spatial and temporal variability of the QC cases. Finally, the conclusions can be found in section 6.

2 Data

For the rain identification study, 8 months (from September 2008- May 2009) of collocated ASCAT 12.5-km Level 2 (L2) wind product, Tropical Rainfall Measuring Mission's (TRMM) Microwave Imager (TMI) rain rate (RR) data, and European Centre for Medium-range Weather Forecasts (ECMWF) winds are analyzed. The ASCAT data in Binary Universal Format Representation (BUFR) are provided by the European Organisation for the Exploitation of Meteorological Satellites (EUMETSAT) Ocean and Sea Ice (OSI) Satellite Application Facility (SAF). They already include ECMWF winds, which are acquired by interpolating three ECMWF 3-hourly forecast winds on a 62.5-km grid both spatially and temporally to the ASCAT data acquisition location and time, respectively. The collocation criteria for TMI rain data are less than 30 minutes distance in time and 0.25° distance in space from the ASCAT measurements. Generally, multiple WVCs are collocated with one rain measurement of TMI. The total amount of collocations is about 17 million, with 15.6 million under rain-free conditions (i.e., TMI RR=0 mm/hr) and 1.4 million under rainy conditions (i.e., TMI RR>0 mm/hr).

To study the quality of ASCAT derived winds and the performance of the improved QC, two different collocation datasets are examined, in which ECMWF winds and buoy winds are used as reference respectively. ECMWF does not well resolve the wind field in the presence of rain [10]. Buoy data are generally more reliable than ECMWF under rainy conditions, although in case of increased wind variability the buoy wind is less representative of an area mean wind such as that of ASCAT. Therefore, in order to better verify the QC approaches, both datasets should have collocated rain data, either satellite derived or in-situ measured RR data.

- The first dataset consists of 15 months (September 2008-December 2009) of ASCAT 12.5-km L2 BUFR data collocated with ECMWF winds and TMI rain data. The total amount of collocations is about 27 million, with 24.6 million under rain-free conditions and 2.4 million under rainy conditions.

- The second dataset consists of three years (March 2009-February 2012) of ASCAT 12.5-km L2 BUFR data collocated with tropical moored buoy wind/precipitation data over the open ocean, and TMI RR data. Since not all the buoys are equipped with a rain gauge, only part of the ASCAT-buoy collocations has rain information. The total amount of collocations in this dataset is about 60 thousand, in which only 3600 contain rain information, either buoy RR parameter or TMI RR data. Note that different rain parameters are only used to identify whether a WVC is rain impacted or not, but not for quantitative analysis. The studied buoys include the National Oceanic Atmospheric Administration (NOAA) Tropical Ocean Atmosphere (TAO) buoy arrays in the tropical Pacific, the Prediction and Research Moored Array in the Atlantic (PIRATA), and the Research Moored Array for African–Asian–Australian Monsoon Analysis and Prediction (RAMA) at the tropical Indian Ocean. Note that buoy wind and rain time series around the collocation time are also used.

3 Singularity analysis

Given a scalar signal s, the singularity exponent (SE) $h(\mathbf{x})$ depicts a dimensionless and scale invariant measure of the degree of local regularity around a given point $\mathbf{x}$. It can be evaluated according to the following function [11],

$$\frac{1}{r}\left|s(\mathbf{x}+r)-s(\mathbf{x})\right| = \alpha(\mathbf{x})r^{h(\mathbf{x})} + o\left(r^{h(\mathbf{x})}\right) \tag{1}$$

where $\alpha(\mathbf{x})$ is a dimensional and signal-dependent amplitude factor, and that the notation $o\left(r^{h(\mathbf{x})}\right)$ means a quantity that decreases to zero faster than $r^{h(\mathbf{x})}$ when r goes to zero. The left part of Eq. (1) is the gradient estimated at half the radius r. Therefore, the singularity exponent roughly behaves as,

$$h(\mathbf{x}) \sim \frac{\log\left|\nabla s(\mathbf{x})\right|}{\log r} \tag{2}$$

Since the presence of long-range correlations in real data can mask the value of $h(\mathbf{x})$, a wavelet projection is used to filter the signal and to provide a stable interpolation scheme in a continuous range of scales. Given a wavelet $\Psi(\mathbf{x})$, the wavelet projection of Eq. (1) becomes

$$\mathrm{T}_{\Psi}\left|\nabla s\right|(\mathbf{x},r) = \alpha(\mathbf{x})r^{h(\mathbf{x})} + o\left(r^{h(\mathbf{x})}\right) \tag{3}$$

So the singularity exponent corresponds to,

$$h(\mathbf{x}) \sim \frac{\log \mathrm{T}_{\psi}\left|\nabla s\right|(\mathbf{x},r)}{\log r} \tag{4}$$

Since we are mainly interested in the most singular structures, the singularity exponents can be estimated in the following way to avoid projecting across multiple scales,

$$h(\mathbf{x}) = \frac{\log\left(\mathrm{T}_{\psi}\left|\nabla s\right|(\mathbf{x},r_0)/\left\langle \mathrm{T}_{\psi}\left|\nabla s\right|(\cdot,r_0)\right\rangle\right)}{\log r_0} + o\left(\frac{1}{r_0}\right) \tag{5}$$

where $\mathrm{T}_{\psi}\left|\nabla s\right|(\cdot,r_0)$ is the mean value of the wavelet projection over the whole signal. The scale r_0 is defined as the smallest accessible scale, i.e., one pixel scale for a discrete 2D image. The numerical implementation of Eq. (5) is described in [12]. Negative singularity exponents derived from Eq. (5) depict that the function is less regular, while the positive values indicate a more regular behavior.

SA can be applied to any satellite-derived image. In this study, SA is applied to ASCAT data. All the ASCAT-derived parameters, such as the σ^0 measurements, the inversion residual (MLE), the measurement variability parameter (i.e., K_p as estimated in [13]), and the retrieved wind components (i.e., U, V, speed and direction) can be used to generate singularity maps. Different

singularity maps are used for different purposes. Thus, SA optimization is required for rain identification.

3.1 Adaption of SA to ASCAT data

In general, the SA algorithm described in [12] works well on ASCAT data. However, it shows in [14] that SA overestimates the irregularity (very negative singularity exponents) of ASCAT measurements at the edge of the swath. A similar effect is found at the edges of non-ocean areas, such as, coastlines, islands, sea ice margin. To overcome such drawbacks, the following processing is performed prior to SA:

a) Within the ASCAT image, the meaningless non-ocean WVC values are replaced by the mean of the input ASCAT parameters over all ocean WVCs within a centered 3x3 box. If the non-ocean WVC is at the corner (or edge) of the image, a closest 2x2 (or 3x2) box is used;

b) The image is extended to the left and right sides of the swath by one node at each row, and the extrapolation point is filled using the mean of ASCAT parameter over all ocean WVCs within the closest 3x2 box (or 2x2 box in case the extrapolation is performed at a swath corner point);

c) The image is also extended before the first row of WVCs and after the last row of WVCs by one point at each column, and the extrapolation point is filled using the mean of ASCAT parameter over all ocean WVCs within the closest 2x3 (2x2 for corner WVCs) box.

Considering the study on ASCAT 12.5-km product, each image consists of ~100x41 WVCs, corresponding to a 3-min long set of WVC rows from one individual swath. Such pre-processing steps remove potential edge artifacts in SA while preserving the information content of the image elsewhere (e.g., singularity fronts associated with rain). As such, SA is applied on the pre-processed image using Eq. (3). And, SE is computed over all ocean WVCs of the original input image.

Due to the noisy nature of the ASCAT parameters (for example over rainy areas), there may be isolated extremely positive or negative SE values after singularity analysis. Therefore, the mean SE value within a centered 3x3 window, i.e., 3x3 WVCs, is taken to generate the final singularity exponent for each WVC. If the ocean WVC is at the corner (or edge) of the image, a closest 2x2 (or 3x2) box is used.

3.2 SA optimization for rain identification

As already mentioned, all the ASCAT-derived parameters can be used to generate singularity maps. In [14], the lowest (most negative) singularity exponents from the singularity maps of the ASCAT zonal (u) and meridional (v) wind components are used to generate the singularity map. Singularities indeed appear in areas of wind convergence or divergence, which represent fronts or downbursts (as observed by ASCAT) that may be associated with rain. In this section, other rain-sensitive ASCAT parameters are assessed before choosing the most optimal singularity maps for rain identification over the ocean surface.

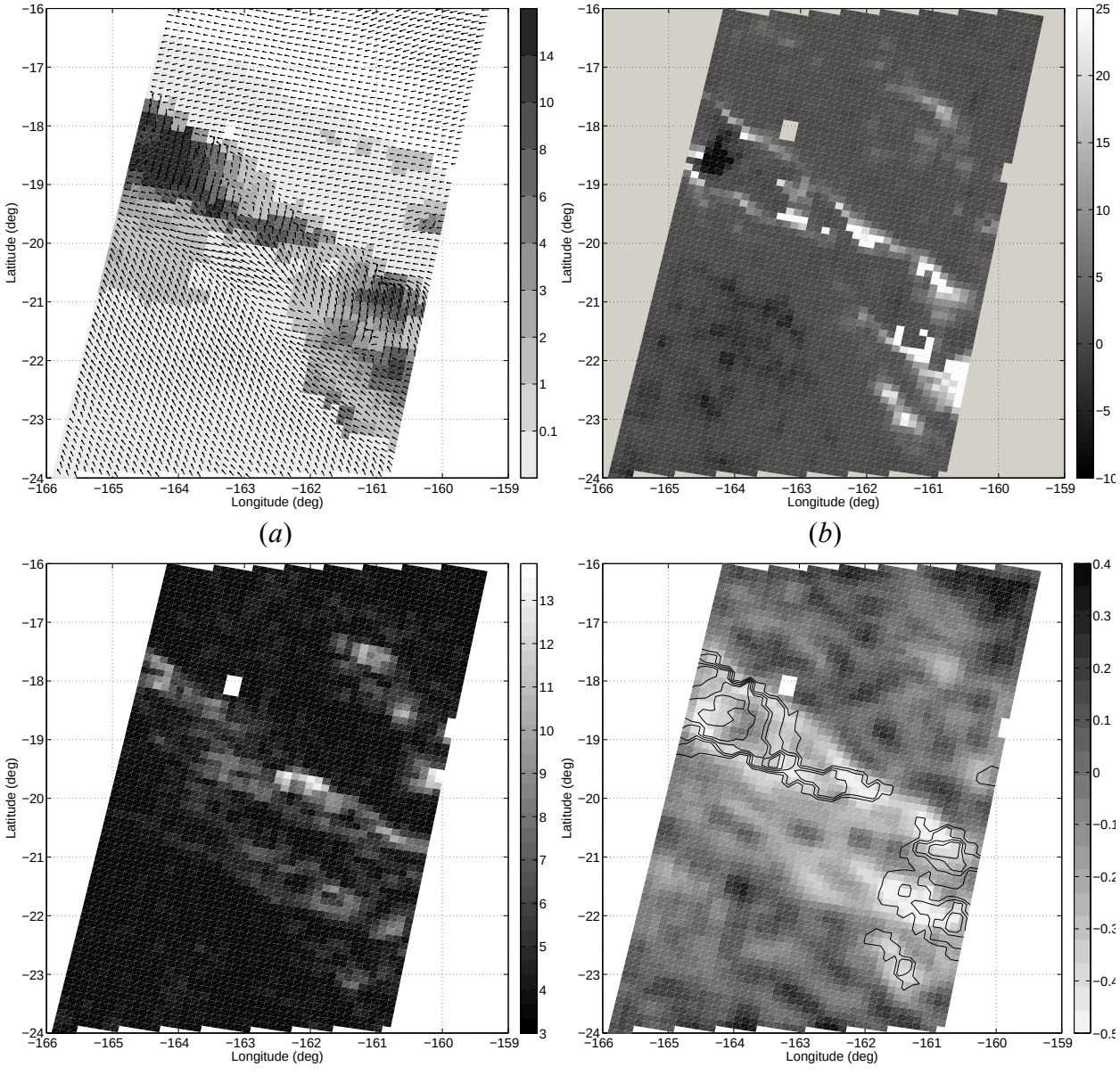

Fig. 1(a) Map of collocated ASCAT-TMI data. The grayscale square areas superimposed correspond to different TMI RRs (see the legend, mm/hr). Note that the white background corresponds to no TMI RR data. The acquisition date was September 24, 2008, at 20:30 UTC; (b) the corresponding MLE distribution and (c) K_p (mean value of fore and aft beams, %) distribution; (d) Singularity map of the ASCAT-retrieved wind field shown in (a). At every grid point, the minimum SE value from the wind speed, wind direction, and MLE SEs is used to generate the map. The RR contour lines depict the rainy areas.

As an example, Figure 1(*a*) shows a particular ASCAT-retrieved wind field (ASCAT 12.5-km product, observed at 20:30 September 24, 2008) with the Tropical Rainfall Measuring Mission's (TRMM) Microwave Imager (TMI) collocated rain rate values superimposed. The collocation criteria for TMI rain data are less than 30 min distance in time and 25 km distance in space from the ASCAT measurements. Typical wind responses, including increased wind variability and wind fronts, are found in the rainy areas. Figures 1 (*b*) and (*c*) illustrate the corresponding MLE and K_p

(i.e., the mean K_p of the fore and the aft beams) values. At low wind speed conditions, the raindrop "splashing" causes additional roughening of the sea surface and in turn an increase of the ocean backscatter from scatterometers. This results in a remarkable increase of the retrieved wind speed. In contrast, at high wind speed conditions, the rain splashing effect is relatively small. Therefore, singularity exponents of the wind speed field can be used to assess the irregularities associated with low wind speed conditions (Fig. 1, areas around [164.5°W 18.5°S] and [161.5°W 21.5°S]). In order to distinguish the wind front associated to the rain-induced flow, SA is then applied on the wind direction field. Singularities can be detected over the sharp transition areas (Fig. 1(*a*), the convergence goes from [164°W 18°S] to [160.5°W 21°S]).

Meanwhile, the rain-impacted ASCAT measurements are generally more inconsistent with the empirical Geophysical Model Function (GMF) than rain-free measurements. This inconsistency results in an increase of the inversion residual and a decrease of the retrieved wind quality. An MLE sign has been defined in [9] to improve the ASCAT MLE-based QC. For low wind speed conditions and in case of heavy rain, the measured σ^0 triplets are generally located outside the cone surface [15] (i.e., negative MLE values) as defined by the GMF. Therefore, the singularity exponent of the MLE field is also examined to better identify rain.

Regarding the measurement variability factor, as the wind variability within a certain WVC increases with rain rate, K_p value increases with RR in general (see the white areas in Fig. 1(*c*)). However, at low wind speed conditions, high K_p value are also found due to the high wind variability (see the area around [161°W 18°S] in Fig. 1(*c*)). Moreover, the estimation of K_p is rather noisy as indicated by the granularity of the K_p map, thus making the rain signature in K_p less evident. As such, the singularity map of K_p is not used in this study.

In this study, singularity maps of the inversion residual and the retrieved wind components (speed and direction) are examined independently for the particular wind field. Then at every grid point, the minimum SE value from the wind speed, wind direction, and MLE SEs is used to generate the final singularity map. Through this approach, the rain-induced wind front and the patchy structure of rainy areas can be detected by singularity analysis simultaneously. Figure 1(*d*) shows the singularity map corresponding to the ASCAT wind and MLE fields shown in Figs. 1(*a*) and 1(*b*). It is also clear that the TMI rain contours in Fig. 1(*d*) well corresponds with the negative SE values. Note that the comparison between SE and TMI RR is intended only to validate the presence of rain, but not the rain rate.

4 SA-based rain flagging results

To estimate the probability of rain (R) $p(R)$ as a function of SE, 8 months (from September 2008-May 2009) of collocated ASCAT 12.5-km product, TMI RR and European Centre for Medium-range Weather Forecasts (ECMWF) winds are explored in this study. ECMWF winds are acquired by interpolating three surrounding ECMWF forecast winds (selected from +3 h to +18 h forecast range in 3-hour steps) on a 62.5-km grid both spatially and temporally to the ASCAT data acquisition location and time, respectively. $p(R)$ is estimated by accumulating two histograms. The first histogram contains the total number of WVCs in the studied category. The second one contains the number of rain-affected WVCs. By dividing the second histogram by the first one, we obtain an estimate of the rain probability.

Figure 2(*a*) illustrates the PDF of $p(SE \mid R)$ (left panel) and the rain probability $p(R \mid SE)$ (right panel) for low wind speeds ($4 \leq V < 6$ m/s). Figure 2(*b*) shows the same plots for high wind speeds ($V \geq 10$ m/s). Two kinds of rain conditions, i.e., TMI-RR>0 mm/hr and TMI-RR$\geq$ 3 mm/hr, are studied. There is an increasing shift of the SE distributions towards negative SE values with increasing RR. The PDF peak of rain-contaminated WVCs is distinct from that of rain-free cases. As noted by the difference between the dashed and the dotted curves in the right panel of Fig. 2(a), the anomalies associated with negative SE values are generally associated with light rain contamination at low wind speeds condition. However, at high winds, such anomalies are associated with heavy rain contamination (see right panel of Fig. 2(*b*)).

For comparison, Fig. 3 shows the same PDFs as Fig. 2 but for the MLE parameter. At low and high wind speed conditions, the extreme (positive or negative) MLE values are generally associated with heavy rain contamination (TMI-RR$\geq$ 3 mm/hr). At low winds, heavy rain contamination is mainly present at large negative MLE values (measurement triplets located outside the cone surface [9]), whereas at high winds, it is present at large positive MLE values (triplets located inside the cone). From the right panels, it seems appropriate to set a MLE threshold to separate rainy cases from rain-free ones. However, since the PDF peaks of rain-free WVCs and rain-contaminated WVCs are quite close to each other (as shown in the left panels, the peaks are around MLE=0), a low MLE threshold will cause substantial false alarm rate.

In contrast, since SE distributions shift considerably with RR (see left panels of Fig. 2), setting a SE threshold can be very effective in filtering rain while keeping a low false alarm rate for low winds.

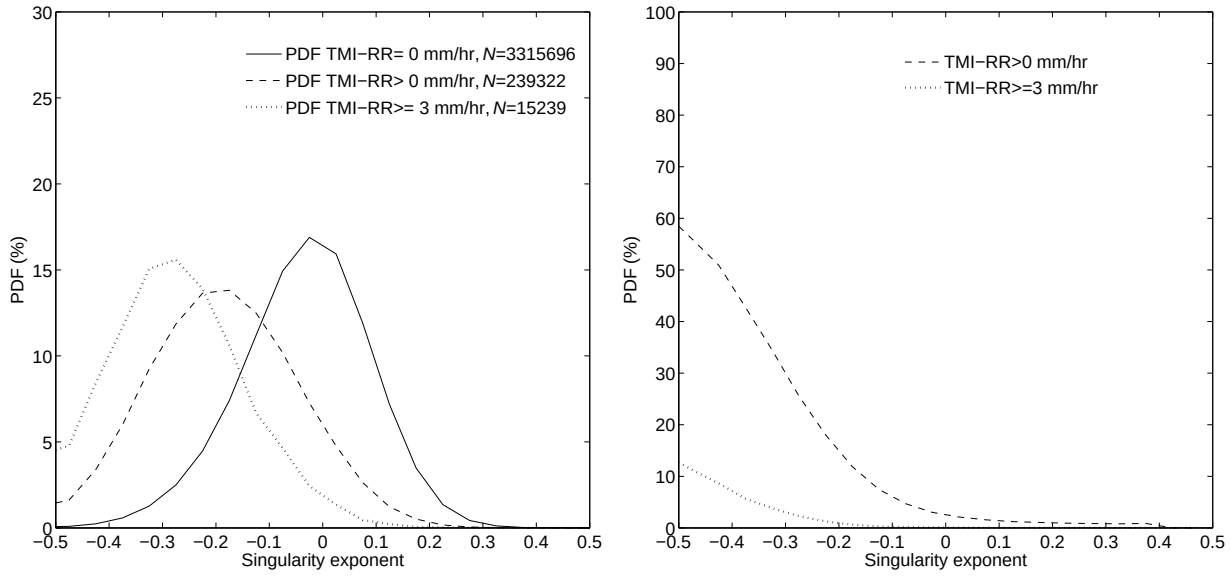

(*a*)

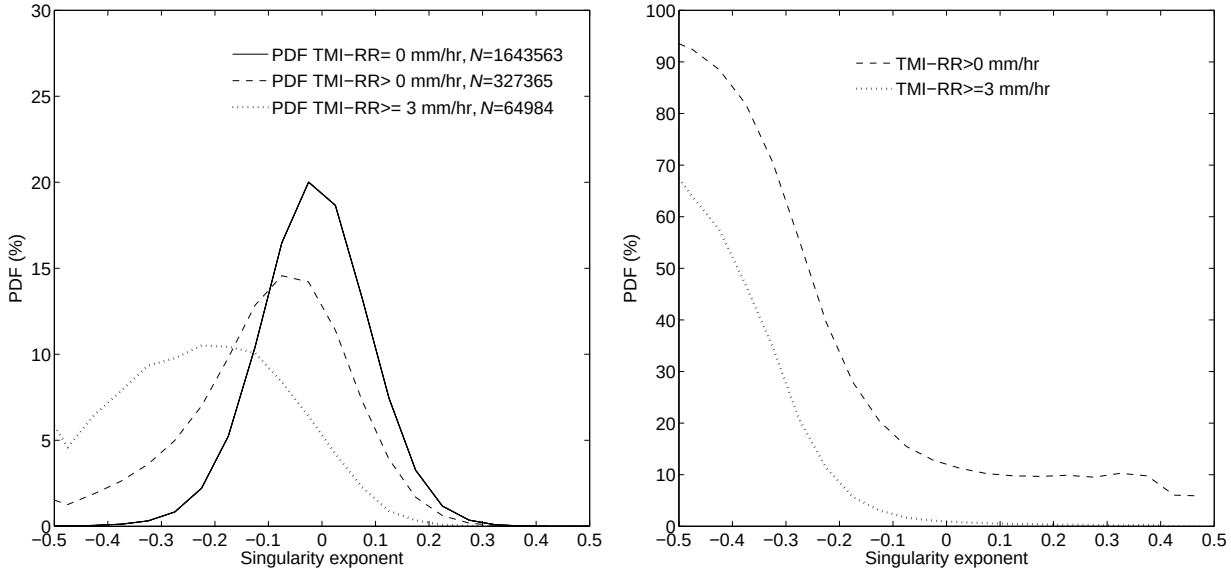

(*b*)

Fig. 2 Illustrations of the PDF of $p(SE \mid R)$ (left panels) and the rain probability $p(R \mid SE)$ (right panels) for (a): low wind speeds (4≤V<6 m/s) and (b): high wind speeds (V≥10 m/s) conditions respectively

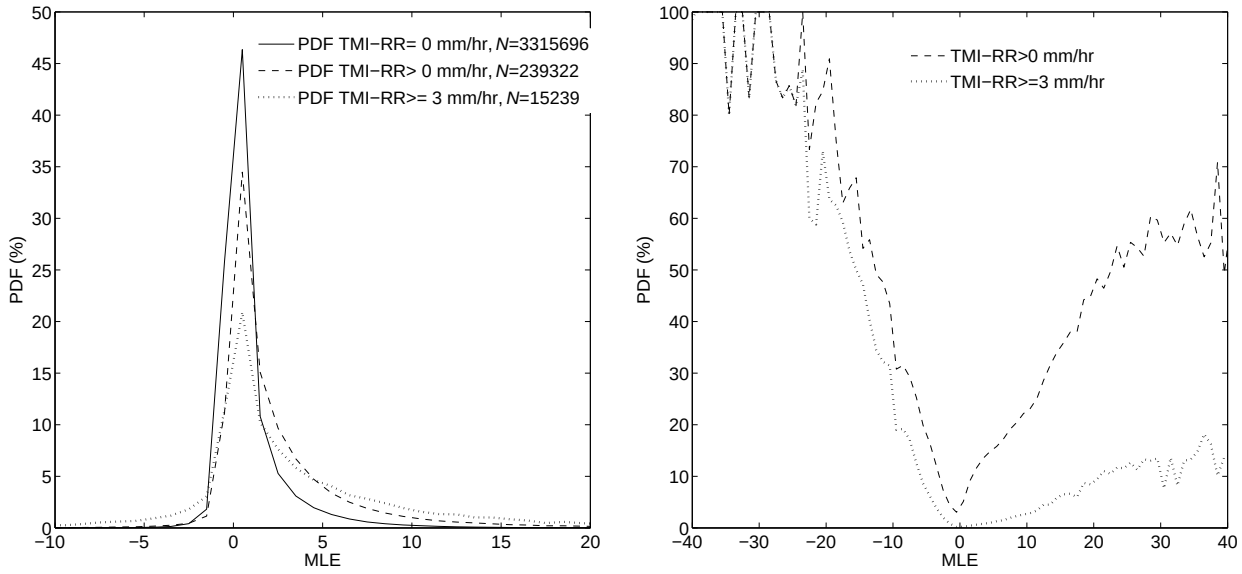

(*a*)

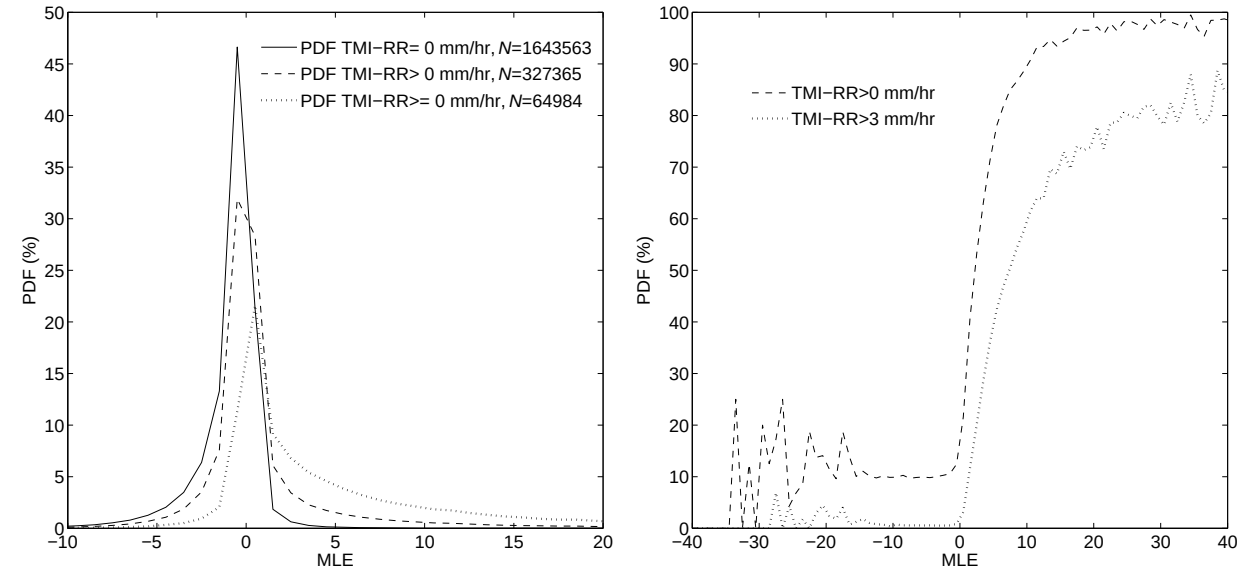

(*b*)

Fig.3 Illustrations of the PDF of $p(MLE \mid R)$ *(left panels) and the rain probability* $p(R \mid MLE)$ *(right panels) for (a): low wind speeds (4≤V<6 m/s) and (b): high wind speeds (V≥10 m/s) conditions respectively.*

Table 1 shows the statistics of SE-based and MLE-based flags respectively. An SE threshold of -0.45 is used, i.e., WVCs with SE<-0.45 are flagged. The threshold of the MLE-based flag is that used in the operational QC, i.e., WVCs with MLE>+18.6 are flagged. For the given thresholds, singularity analysis flags a bit more rain-contaminated WVCs than MLE. However, the latter flags slightly more heavy rain contaminated cases than SA. Another interesting result is that WVCs

flagged by MLE-based filter and WVCs flagged by SE-based filter do generally not coincide (coincidence ratio less that 20% for the given thresholds in table 1), indicating that SE is not only a good rain indicator but also very complementary to the operational MLE-based QC. The VRMS differences between the ASCAT winds and the ECMWF winds are also presented in the table. It shows that low SE values also correlate well with high VRMS scores. Note though that [10] has shown that ECMWF winds show poor verification in rainy areas and are thus a poor proxy for ASCAT wind data quality.

Note that both flags filter a small portion of apparent poor-quality WVCs (i.e., large VRMS values) in the absence of rain. These ASCAT-derived winds are affected by increased local wind variability, confused sea state, and/or radar footprint contaminated by land or ice, which increase the measurement variance, and lead to large discrepancies between the measured triplets and the GMF (i.e., high MLE values), and low negative SE values. In the presence of rain, the associated rain splash and wind downbursts may change the characteristics of the SE and MLEs and which is the focus of this section. In the next section, SA will be further explored for QC purposes. Moreover, further experiments will be carried out to determine whether ASCAT wind quality degradation is dominated by increased wind variability or rain contamination effects.

Table 1. Statistics of the ASCAT rain flagging using the singularity analysis (SE threshold: -0.45) and the operational MLE-based (MLE>+18.6) methods. The second and third rows show the vector root-mean-square (VRMS) differences between the ASCAT winds and the ECMWF winds. The last two rows present the percentage of flagged WVCs contaminated by rain, according to different TMI RR intervals.

	SE	MLE
Flagging ratio (%)	0.42	0.31
VRMS, Non-flagged (m/s)	2.28	2.28
VRMS, flagged (m/s)	5.91	6.07
% of flagged WVCs with TMI-RR>0 mm/hr	82.3	72.7
% of flagged WVCs with TMI-RR≥ 3 mm/hr	44.5	46.0

5 SA-based complementary QC

In section 4, the SA method has been further developed for the optimization of ASCAT rain identification [16]. It turns out that SA is sensitive to increased inter-WVC wind variability at very local scales (mostly within the nearest neighbor WVCs), generally associated with rain events and frontal structures. Due to the large spatial variability of rain, SA is proven to be more effective than MLE in terms of exploiting the rain signatures present in ASCAT parameters, especially for the lower rain rate and low wind conditions, where the MLE is less sensitive to these cases. As a result, SA mostly detects rain-contaminated WVCs when the MLE-based QC does not, and vice versa, indicating that these two techniques are very complementary for the purposes of both rain detection and quality control.

Using spatial derivatives (like in SA) is however potentially detrimental, as steep wind gradients may be removed, while particularly relevant for some applications. This poses a challenge in verification of the QC scheme as spatial and temporal representativeness are dominating the quality indices. Moreover, where rain is spatially erratic, it induces downbursts of wind on the ocean surface with strong gust fronts and as such rain is associated with enhanced wind variability. Wind verification of a QC scheme by buoy data thus may be penalizing conditions with such high wind variability, since the wind vector measured at a buoy location is generally expected to differ much from the scatterometer wind in case of high wind gradients. Equally, [10] has shown that the European Centre for Medium-range Weather Forecasts (ECMWF) winds show poor verification in rainy areas and are thus a poor proxy for ASCAT wind data quality. Another inherent problem in scatterometer wind processing near steep gradients resides in the ambiguity removal [17], which is most challenging in variable wind conditions.

In this section, the SA is further adapted and tested for QC purposes. A complementary approach using both singularity exponent (SE) and MLE is proposed to improve the current ASCAT QC. Section 5.1 identifies and describes the quality-sensitive parameters, including MLE, the measurement variability factor K_p, and the singularity exponent (SA output), independently. A measure of ASCAT wind quality is presented as a function of each mentioned parameter. Here, the VRMS difference between ASCAT and ECMWF winds is used as a quality indicator. In section 5.2, a complementary QC approach using SE and MLE is firstly proposed to improve the current ASCAT wind QC. This approach can be further improved by analyzing its performance in separate wind speed and K_p categories, leading to the development of a multi-dimensional histogram (MUDH) technique. Section 5.3 evaluates the performances of the proposed QC approaches using collocated ASCAT data and buoy winds, taking account of the enhanced local spatial and temporal variability of the QC cases.

5.1 Quality-sensitive parameters

This section describes three ASCAT quality-sensitive parameters separately. The goal is to see general trends in data quality. Buoy data is too scarce to show parameter sensitivity to rain and data quality. Thus the VRMS difference between ASCAT and ECMWF winds is presented as a function

of each parameter for different wind speed and rain conditions, in order to better understand the sensitivity of each parameter to the wind quality. As already mentioned in section 4, note that although the ASCAT wind retrieval quality is known to be somewhat degraded under large small-scale wind variability and heavy rain conditions, [10] shows that the ECMWF winds do not resolve at all such conditions. As such, discrepancies between ASCAT and ECMWF can be mainly attributed to the ECMWF model not representing the local convective features. Wind speeds below 4 m/s are not considered in this study, since low winds generally correspond to high wind variability and poor wind direction skill, which makes the analysis much more challenging, i.e., beyond the scope of this study.

5.1.1 MLE

For ASCAT, the wind inversion is implemented by searching for the minimum distance between the backscatter triplet and the GMF in a transformed 3-dimensional (3D) measurement space (namely z-space), i.e., the following MLE function is minimized [15],

$$MLE = \frac{1}{3}\sum_{i=1}^{3}\left(z_{mi} - z_{si}\right)^2 \tag{6}$$

where $z_{mi} = \left(\sigma_{mi}^0\right)^{0.625}$ is the backscatter measurement of the *i*th beam in z-space, and $z_{si} = \left(\sigma_{si}^0\right)^{0.625}$ is the backscatter simulated through the GMF, i.e., CMOD5n [18], using the solution wind vector as input. In general, the ASCAT backscatter triplets are close to the GMF, corresponding to low inversion residuals or MLE values. To account for noise, the expectation value of the MLE is normalized to one [19]. Occasionally, a large inconsistency with the GMF is induced by geophysical conditions that are not modelled by the GMF, such as increased local wind variability, confused sea state, rain, or land/ice contamination, resulting in large MLE values. Consequently, the MLE is a good indicator of the retrieved wind quality in a WVC. An MLE sign is defined in [9] to improve the MLE-based QC. The sign works as follows: triplets located inside the cone surface constructed by the GMF in measurement space [15] are assigned with a positive MLE value, while those located outside the cone are assigned with a negative MLE value. The MLE is generally a proxy for WVC wind variability, where negative MLEs denote stable flows and positive MLEs unstable flows. Excessive positive MLEs are generally found near (gust) fronts, squall lines and convective systems.

Figure 4 shows the mean VRMS difference between ASCAT and ECMWF winds as a function of MLE for different wind speed regions at rain-free and rainy conditions respectively. There is a clear distinct behaviour for MLE values in terms of wind quality in both panels. Under rain-free conditions, ASCAT winds retrieved from the triplets inside the cone (associated with positive MLE values in Fig. 4(*a*)) increase rapidly in VRMS difference as the triplet's distance to the GMF increases. However, for the triplets outside the cone (associated with negative MLE values), the wind VRMS difference is generally small regardless the triplet's distance to the cone. In line with this, the current MLE-based QC which uses a threshold of +18.6 to filter poor-quality WVCs works well for the measurements under rain-free condition [9]. Under rainy conditions, ASCAT winds above 4 m/s have rapidly increasing VRMS difference (w.r.t. ECMWF) as the triplet's distance to the cone increases, regardless the triplet's location. The apparent quality degradation toward

negative MLE values is especially sharp for wind speed region of [4 7) m/s. This may be understood from the fact that stable flow (negative MLE) will be associated with relatively dry air descending from the rain clouds and spreading over the ocean, which process is not resolved by the ECMWF model, thus leading to large VRMS differences in rainy areas. Another reason could be due to triplets that are moved away from the cone due to rain contamination.

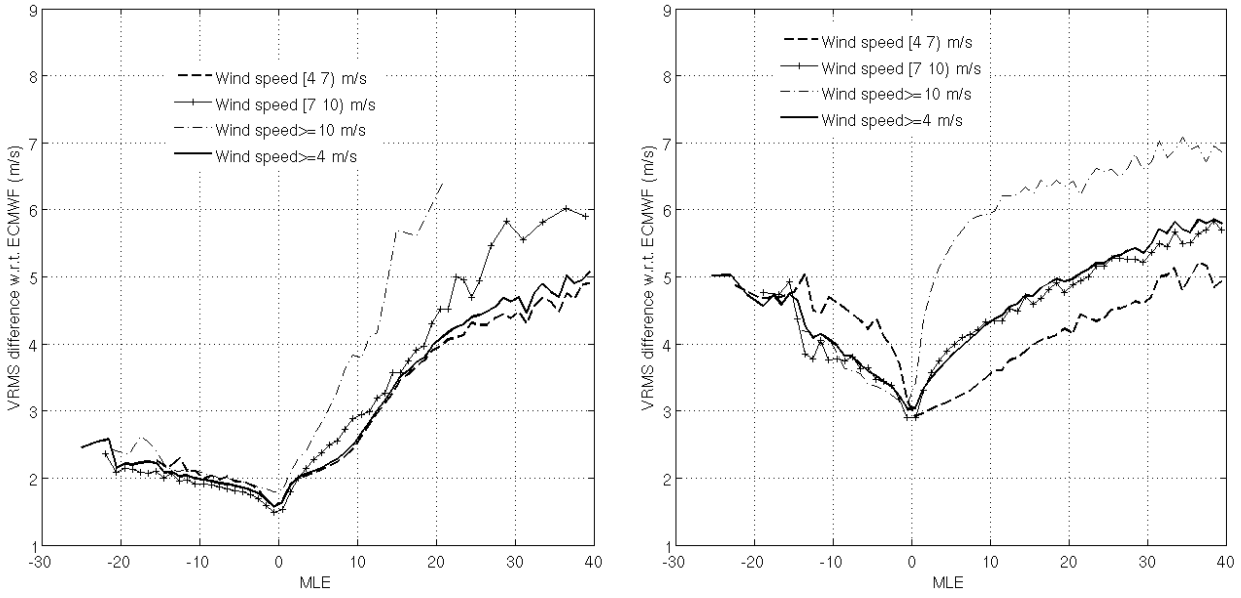

Fig. 4. Mean VRMS difference between ASCAT and ECMWF winds as a function of MLE for (a) TMI rain-free collocated WVCs and (b) TMI rain-contaminated WVCs. The MLE binning is set to be 1. In case that the number of collocations in a studied bin is less than 100, the bin is merged with its closest bin.

The VRMS differences of the current MLE-based QC are summarized in table 2. As discussed in [9], on the one hand, large positive MLE values correspond to increased sub-WVC variability and in turn somewhat degraded ASCAT-retrieved wind quality; on the other hand (and as already discussed), increased small-scale wind variability is not resolved at all by ECMWF. VRMS scores are consequently high. Therefore, the table mainly indicates the degraded quality in ECMWF winds in case of ASCAT QC. The total scores of the operational QC are presented in the last row of table 2. Regarding that ~10% of the collocations are with RR>0 mm/h, it is evaluated that more than two thirds of QC-ed WVCs are in convective areas with rain. Especially, more than 90% of QC-ed WVCs are in variable wind conditions near rain for the cases with wind speeds ≥ 7 m/s, indicating that convection is the main factor in complicating ASCAT wind verification under these high wind conditions in the tropics.

Table-2: Percentage and mean VRMS difference (m/s) between ASCAT and ECMWF winds for QC-accepted and rejected data for different wind speed regions and rain conditions.

Wind speed(m/s)	TMI rain free			TMI rain contaminated			TMI all weather conditions		
	VRMS-Kept	VRMS-Rejected	QC-ed ratio(%)	VRMS-Kept	VRMS-Rejected	QC-ed ratio(%)	VRMS-Kept	VRMS-Rejected	QC-ed ratio(%)
[4 7)	1.72	4.42	0.18	3.07	4.68	2.18	1.81	4.54	0.31
[7 10)	1.55	5.65	0.04	3.19	5.59	3.10	1.68	5.60	0.29
≥ 10	1.84	8.40	0.02	3.64	6.90	2.16	2.12	6.95	0.36
≥ 4	1.67	4.69	0.10	3.28	5.65	2.51	1.80	5.37	0.31

5.1.2 Singularity exponent

Since the MLE is generally a proxy for sub-WVC wind variability where large positive MLEs are generally found near (gust) fronts, squall lines and convective systems, one might expect that the MLE and SE values are inversely proportional and thus redundant. However, note that the MLE is a local measure, whereas SE is based on spatial derivatives between WVCs and therefore may indeed be complementary to MLE values.

Figure 5 shows the mean VRMS difference between ASCAT and ECMWF winds as a function of the SE value derived from section 3. ECMWF winds are less representative of ASCAT winds as the SE value decreases, which is in line with the general smoothness of the ECMWF model near convection [10]. The apparent quality degradation rate is larger at high wind speeds than that at low wind speeds, as the former implies deeper convection. Another interesting result is that WVCs flagged by MLE-based filter and WVCs flagged by SE-based filter with a threshold of -0.45 do generally not coincide (45% of the operationally QC-ed WVCs are with SE<-0.45; while 32% of the WVCs which correspond to SE<-0.45 are with MLE>+18.6), indicating that SE is potentially very complementary to the operational MLE-based QC. In section 5.2, SE is further used to complement the current MLE-based QC. Then, a more comprehensive study using SE, MLE, K_p and wind speed is developed to refine the complementary QC approach.

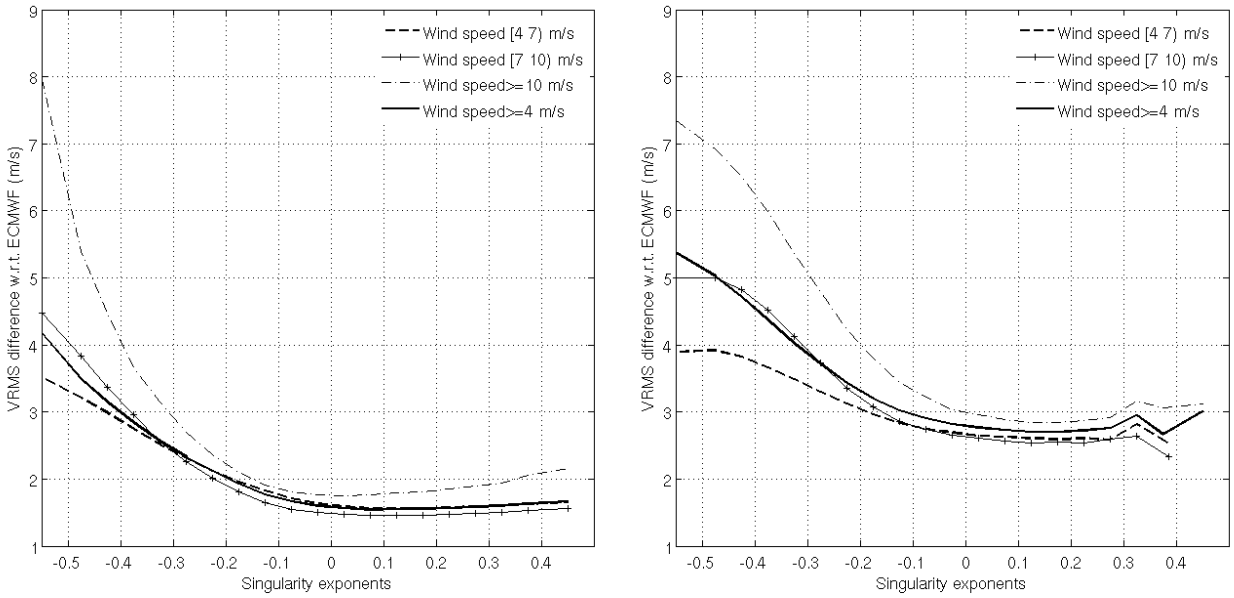

Fig. 5. Mean VRMS difference between ASCAT and ECMWF winds as a function of SE (bins of 0.05) for (a) TMI rain-free collocated WVCs and (b) TMI rain-contaminated WVCs.

5.1.3 Measurement variability factor (K_p)

The variability of ASCAT backscatter σ^0, namely K_p, is defined as the normalized standard deviation of the measurements, i.e.,

$$K_p = \frac{\sqrt{\mathrm{var}(\sigma^0)}}{\overline{\sigma^0}} \tag{7}$$

where $\overline{\sigma^0}$ is the mean backscatter of a beam in a WVC and $\mathrm{var}(\sigma^0)$ is its estimated variance . The K_p value can be regarded as a measure of the error in the mean backscatter caused by speckle noise, instrument characteristics, data processing, and spatial heterogeneities of the target [13], such as wind variability.

Similar to Fig. 4, the behaviour of K_p in terms of wind VRMS difference is shown in Fig. 6 for rain-free and rainy conditions separately, in which the horizontal axis indicates the mean K_p value of the fore and aft beams. As expected, the VRMS wind difference generally increases as the measurement error increases. The apparent wind quality degradation rate in Fig. 6 is smaller than that in Fig. 4, except for wind speeds ≥ 10 m/s under rain conditions. This indicates that K_p may be helpful to detect spatially variable weather conditions. In section 5.2.2, K_p is adopted by the MUDH QC algorithm to improve the filtering of poor-quality winds.

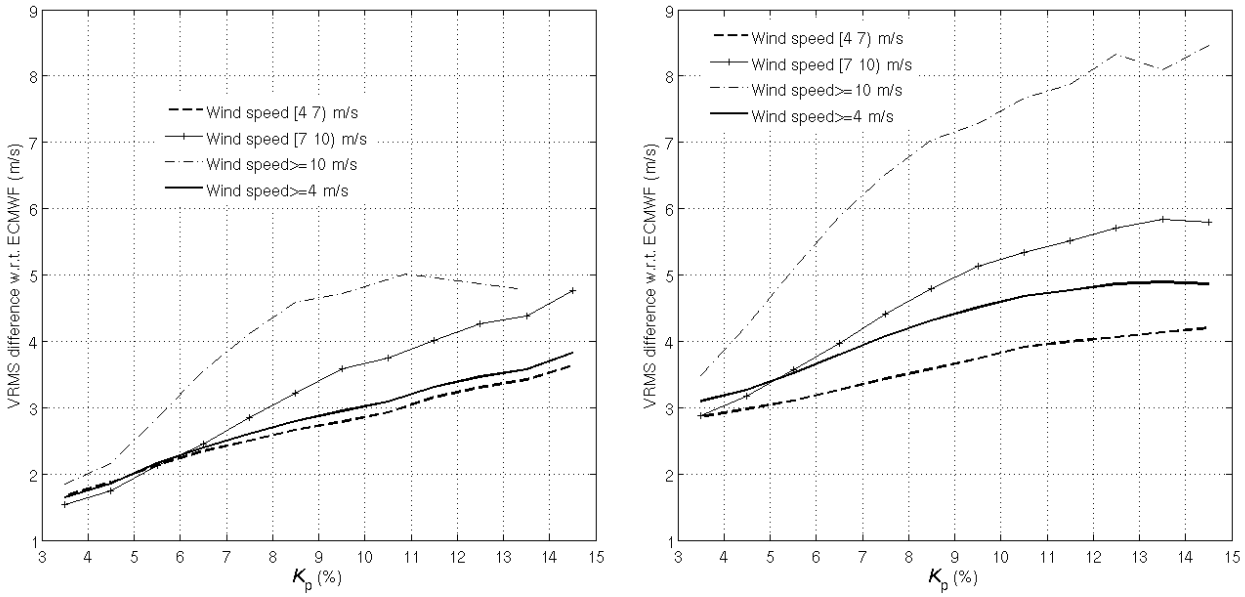

Fig. 6. Mean VRMS difference between ASCAT and ECMWF winds as a function of K_p (bins of 1%) for (a) TMI rain-free collocated WVCs and (b) TMI rain-contaminated WVCs.

5.2 Improved QC methods

Although the VRMS difference between ASCAT and ECMWF is not necessarily a good indication of ASCAT quality, it does indicate extreme wind variability and convection, where SE (as MLE) may be effective in detecting unrepresentative ASCAT winds, and it is therefore used below. This section presents two approaches to improve the single parameter (MLE-) based QC. The first one is based on a combination of the singularity exponent and the MLE. The second methodology uses all the mentioned quality-sensitive parameters in Section 5.1 (including SE, MLE, K_p and wind speed) to develop a Multi-dimensional Histogram (MUDH) QC flag. The idea behind these two approaches is as follows: the mean VRMS difference between ASCAT and ECMWF winds is estimated in a 2-D (first approach) or 4-D (second approach) space. Then a flag table is derived by setting the 2-D or 4-D bins which VRMS difference is higher than the threshold T_{vrms} to be flagged, and setting the bins which VRMS difference is lower than T_{vrms} to be unflagged. Note that we do not intent to perform QC for WVCs with MLE value less than +18.6 and SE value larger than -0.2. Due to the lack of data in certain bins, the corresponding VRMS values may be extremely high or low, leading to isolated flag bins in the table. A neighbour filtering is then applied to the flag table. If the number of data in a certain bin is higher than 50, its corresponding flag value is kept. Otherwise, if the mean VRMS of this bin is above the threshold value T_{vrms}, the bin is initially set as QC flagged. Then, the number of adjacent bins within a 3x3 box which are set to filter data is accounted for. If more than half of the adjacent bins are set as QC flagged, we consider it to be sufficient evidence for filtering winds associated with this bin, or else we leave the flag unset for this bin. Finally, the processor simply uses the derived quality-sensitive parameters, converts them into table indices, and checks for the corresponding bin value in the flag table.

5.2.1 Combined SE/MLE approach

As introduced in [16] and mentioned in section 5.1.2, SE is complementary to MLE in terms of quality control. Figure 7(*a*) shows the mean VRMS difference as a function of SE and MLE for wind speeds above 4 m/s. The white areas are due to the lack of data in the corresponding bins, in which the number of collocations is less than five. It is consistent with the established fact that ASCAT wind quality generally decreases as the MLE value increases and it shows increased VRMS differences as the SE value decreases. Large VRMS differences occur for a set of ASCAT winds derived from triplets that are close to the GMF cone surface (low absolute MLE value and low SE value) that are now detected by the combined analysis, but which have not been examined before.

A threshold of T_{vrms}=4.5 m/s is used to produce the flag table (see Fig. 7(*b*)). To inherit the current QC, WVCs with MLE above +18.6 are always rejected. The dark gray corresponds to the bins set for filtering (QC-rejection criterion), while the light gray corresponds to the bins unset for filtering (QC-acceptance criterion). A verification of this QC approach is summarized in table 3. When compared with the MLE-based QC statistics in table 2, it is clear that in general the new algorithm is rejecting more points than the MLE-based QC. By construction, the VRMS scores for filtered data are comparable in both algorithms, since VRMS differences will be large for low SE mainly due to the large spatial representativeness error of the ECMWF winds near convection. Therefore, the new algorithm filters many more winds near rain at low and moderate wind speed (v<10 m/s) categories. For wind speeds below 10 m/s, the VRMS scores of filtered WVCs are slightly lower than those filtered by the MLE-based QC, while for wind speeds above 10 m/s, the VRMS scores are higher.

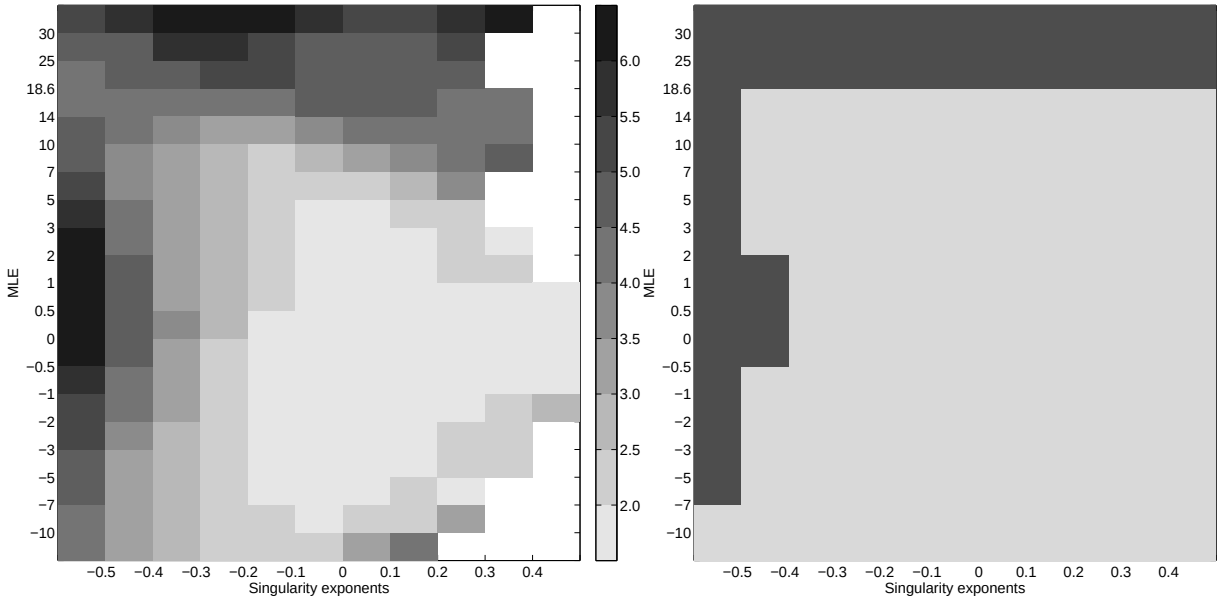

(*a*) (*b*)

Fig. 7. (a) Mean VRMS difference between ASCAT and ECMWF winds as a function of SE and MLE. The blank area is due to the lack of data in the corresponding bins. The grayscale corresponds to different VRMS values (see the legend). (b) A simple QC flag table derived from (a). The dark gray corresponds to the bins set for filtering (QC-rejection criterion); the light gray corresponds to the bins unset for filtering (QC-acceptance criterion).

Table-3: Percentage and mean VRMS difference between ASCAT and ECMWF winds for QC-accepted and QC-rejected WVCs using the combined SE/MLE flag table in Fig. 7.

Wind speed(m/s)	TMI rain free			TMI rain contaminated			TMI all rain conditions		
	VRMS-Kept	VRMS-Rejected	QC-ed ratio(%)	VRMS-Kept	VRMS-Rejected	QC-ed ratio(%)	VRMS-Kept	VRMS-Rejected	QC-ed ratio(%)
[4 7)	1.71	4.03	0.33	3.03	4.47	5.02	1.80	4.26	0.64
[7 10)	1.54	4.83	0.09	3.12	5.53	5.74	1.67	5.43	0.55
≥ 10	1.83	7.13	0.06	3.56	7.35	3.94	2.10	7.34	0.69
≥ 4	1.66	4.32	0.19	3.22	5.58	4.97	1.79	5.22	0.61

The rain impact on VRMS wind difference can also be understood using the combined SE/MLE analysis. Figure 8 shows the mean TMI RR as a function of SE and MLE value. Similar to the VRMS difference between ASCAT and ECMWF winds, the mean TMI RR increases as the triplet's distance to the cone surface increases and the SE value decreases, indicating that more rain is present for both high sub-WVC variability (MLE) and high inter-WVC variability (low SE). In fact, as shown in section 5.3.2, high inter-WVC variability implies high sub-WVC variability and SE is complementary to MLE. So, high rain rates associate well with small SE values and large MLE values.

One should also note that the distribution of large mean TMI RR in Fig.8 does not align exactly with the VRMS score in Fig. 7.The VRMS differences in Fig. 7 are most likely due to the local increase of wind variability, which is mostly associated with rain events. However, as already mentioned, ECMWF does not well resolve the ocean wind field under rainy conditions. As such, other independent and reliable wind sources, such as buoy winds, should be used to assess the ASCAT wind quality in the presence of rain (see section 5.3).

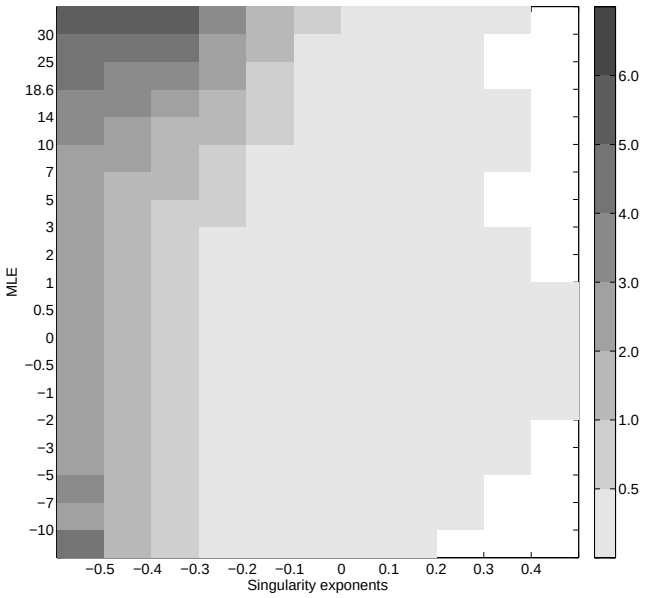

Fig. 8. The mean TMI RR as a function SE and MLE. Only the collocations with wind speeds above 4 m/s are used.

5.2.2 MUDH approach

To refine the QC approach introduced in Section 5.2.1, an extended analysis is presented in this section by also taking the measurement variability (K_p) and wind speed parameters into account, leading to the development of the Multidimensional Histogram (MUDH) technique. MUDH was first developed in the context of scatterometry to flag rain contamination for SeaWinds on QuikSCAT [1]. It identifies parameters that are sensitive to rain, estimates the probability of rain as a function of them using a training data set, and then uses the rain probability to flag for rain. MUDH is adapted here to improve ASCAT QC. As such the VRMS difference between ASCAT and ECMWF winds, instead of the rain probability, is estimated during the development of MUDH for ASCAT. Then, a VRMS threshold introduced before is used to flag data.

Figure 9 illustrates the ASCAT VRMS scores as a function of SE and MLE for the categories of moderate wind speed/small K_p value, moderate wind speed/large K_p value, high wind speed/small K_p value, and high wind speed/large K_p value respectively. The white areas are due to the lack of data in the corresponding bins (number of data <5). The behavior of SE and MLE in terms of wind VRMS difference clearly varies with K_p and wind speed. On the one hand, the causes for increased VRMS scores are different for each category. For instance, convection is the main cause of apparent quality degradation for the category of high wind speed and large K_p value, in which the mean rain rate is generally higher than 3 mm/h (not shown) over all the SE/MLE bins and thus more convective activity is present. Since the winds are high, the large VRMS value is not likely due to rain splash, but more likely due to large ECMWF errors and sub-WVC wind variability effects on ASCAT-retrieved quality. The large VRMS distributions in Fig. 9(*b*)-(*c*) are also associated with relatively high mean TMI RR (not shown). However, the mean TMI RR is really low for the category of low wind speed and small K_p value (less than 0.5 mm/h for all the SE/MLE bins, except for those bins in the left lower corner of Fig. 9(*a*)). Also here the elevated VRMS scores may be caused by increased local wind variability. On the other hand, the rain splash produces different effects on MLE for different wind speed conditions. Apparent poor-quality winds induced by rain are generally associated with low negative MLE values under low wind speeds (see the lower left corner of Fig. 9(*b*)), and associated with only small effects at high wind speeds.

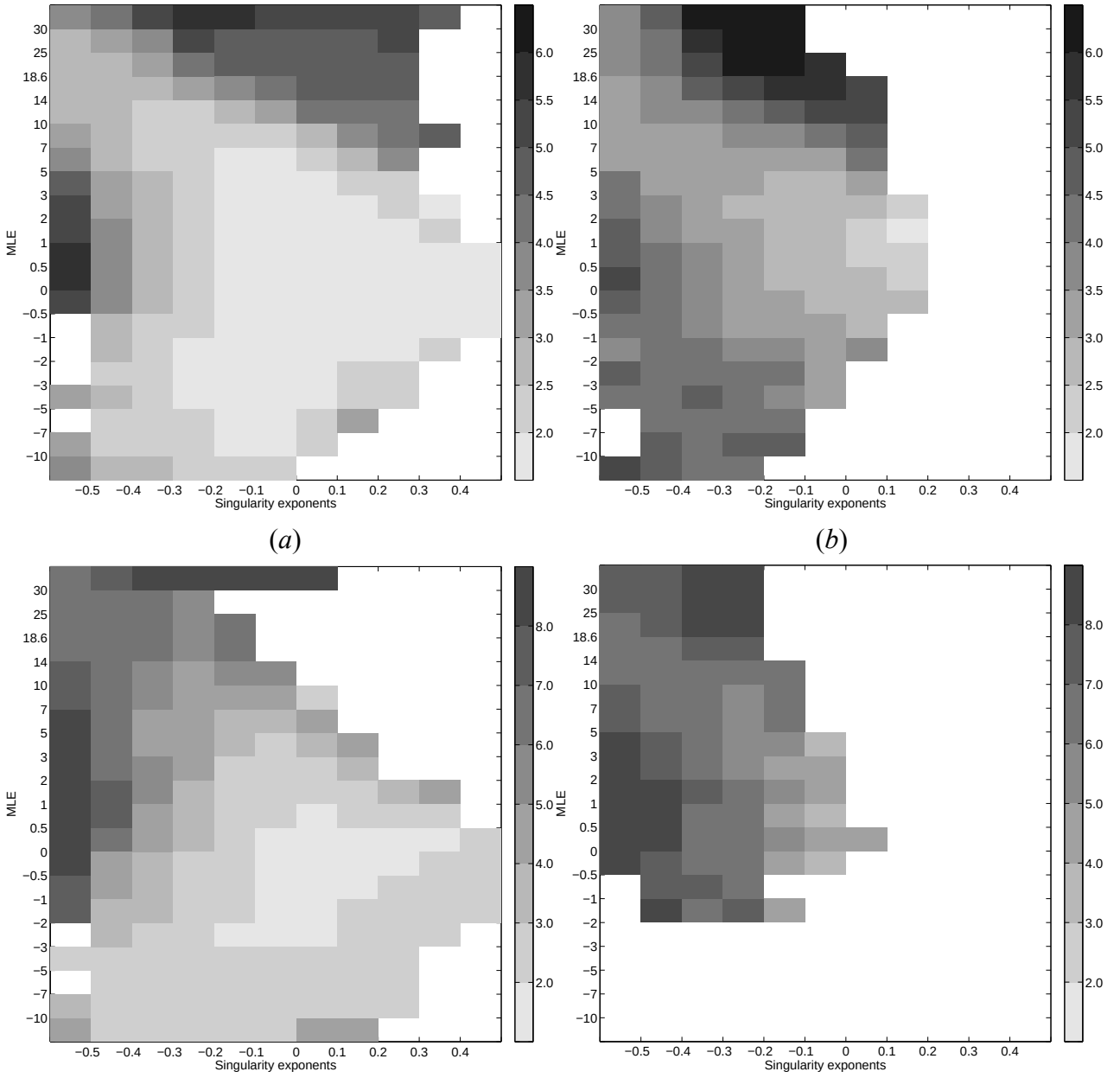

Fig. 9. Mean VRMS difference between ASCAT and ECMWF winds as a function of SE and MLE for (a) moderate wind speeds (4≤v<7 m/s) and small K_p values (K_p<4%); (b) moderate wind speeds (4≤v<7 m/s) and large K_p values (K_p>7%); (c) high wind speeds (v>10 m/s) and small K_p values (K_p<4%); and (d) high wind speeds (v>10 m/s) and large K_p values (K_p>7%). The gray scale indicates the VRMS values (see the legend); the blank area is due to the lack of data in the corresponding bins.

To implement the MUDH QC approach, the binning of MLE and SE are set according to the axis labels of Fig. 9. The wind speeds are roughly separated into three categories, i.e., 4≤v<7 m/s; 7≤v<10 m/s; and v≥10 m/s. The K_p (mean value of the fore- and aft-beams) bins are set as follows: K_p<3%, K_p≥15%, and bins of 2% for K_p in the range [3% 15%). Since the VRMS scores depend on

wind speed, a set of thresholds T_{vrms}=4.0, 4.4, and 6.2 m/s are used for the wind speed categories $4 \le v < 7$ m/s, $7 \le v < 10$ m/s, and $v \ge 10$ m/s, respectively, in order to produce the multi-dimensional QC flag table and account for the variable ECMWF errors. A verification of the MUDH technique on ASCAT QC is summarized in table 4, which can be compared to that of the MLE-based QC (table 2) and the SE/MLE QC (table 3). It shows that the MUDH technique filters nearly three times as many WVCs as the MLE-based QC and 50% more than the SE/MLE QC, while the VRMS difference of the filtered WVCs is similar for the three QC techniques. Similar conclusions can be drawn when splitting the analysis into different wind speed categories. Moreover, MUDH filters many more ASCAT measurements in variable wind areas with rain, especially for wind speeds below 7 m/s.

Table-4: Percentage and mean VRMS difference between ASCAT and ECMWF winds for QC-accepted and rejected data using the MUDH algorithm.

Wind speed(m/s)	TMI rain free			TMI rain contaminated			TMI all rain conditions		
	VRMS-Kept	VRMS-Rejected	QC-ed ratio(%)	VRMS-Kept	VRMS-Rejected	QC-ed ratio(%)	VRMS-Kept	VRMS-Rejected	QC-ed ratio(%)
[4 7)	1.71	3.96	0.44	2.98	4.49	8.32	1.79	4.26	0.96
[7 10)	1.54	4.61	0.13	3.04	5.63	8.38	1.66	5.48	0.80
≥ 10	1.83	7.00	0.08	3.52	7.35	5.02	2.10	7.32	0.88
≥ 4	1.66	4.22	0.26	3.16	5.53	7.39	1.78	5.17	0.88

5.3 Validation results

5.3.1 Validation with 10-min buoy wind measurements

As discussed in section 5.2, in [10] Portabella et al show that ECMWF does not well resolve the rain-induced wind flow and, as such, is not a reliable wind reference for assessing the ASCAT QC in the presence of convection. To better assess the performance of the proposed complementary QC algorithms, an independent wind source, such as buoy data, is required. However, since the number of ASCAT-buoy collocations (especially those with rain information) is much smaller than that of ASCAT-TMI collocations, it is not possible to make an as thorough analysis as in section 5. Consequently, a set of larger MLE bins is used in this section.

Figure 10(*a*) shows the VRMS difference between ASCAT and buoy (solid), ASCAT and ECMWF (dashed), for the collocations of the second data set (ASCAT-ECMWF-Buoy), as introduced in Section 2. It confirms that WVCs with the most negative singularity exponents are in areas with large wind variability, as expected. The dash-dotted line associated to the right y-axis shows the percentage of rainy collocations with RR ≥ 3 mm/h. As before, high probability of rain is found for the most negative singularity exponents indicating high WVC variability. In general, the reduced correspondence of buoy, ASCAT and ECMWF winds with decreasing SE values is further confirmed. Figure 10(*b*) presents the VRMS difference between ASCAT and buoy winds as a function of SE and MLE. It shows a similar pattern to that in Fig. 7(*a*), which again indicates that SE and MLE parameters are complementary in terms of quality control.

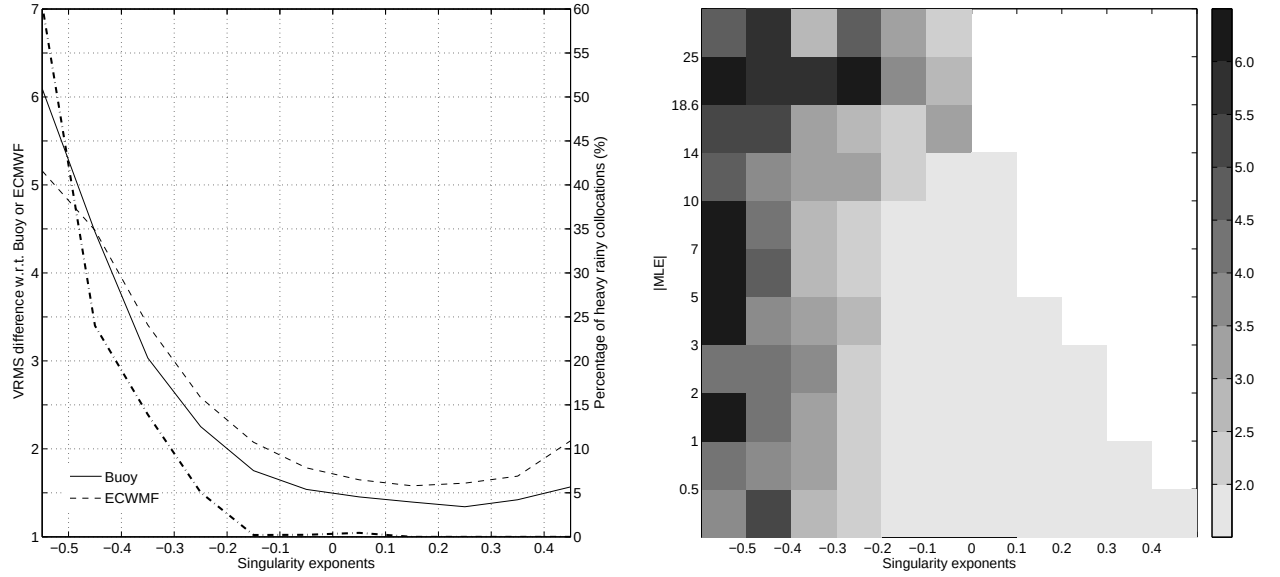

(*a*) (*b*)

Fig. 10. (a) The VRMS difference between ASCAT and buoy winds (thin solid); ASCAT and ECMWF winds (dashed); the dash-dotted line shows the percentage of rain contaminated WVCs (TMI RR or averaged 2-hourly buoy RR ≥ 3 mm/h) in each bin for the 3000 ASCAT-buoy collocations with rain information; (b) the mean VRMS difference between ASCAT and buoy winds as a function of SE and MLE.

Table 5 presents the QC results of the collocated ASCAT-buoy data set using the three mentioned methods, i.e., the current MLE-based QC (threshold of +18.6), the combined SE/MLE analysis, and the MUDH technique. Regarding the complementary QC approaches, the flag tables derived in Section 5.2 (using collocated ASCAT-ECMWF-TMI dataset) are used to filter the dataset with collocated ASCAT-buoy measurements. Buoy winds are adopted as reference in the statistics.

The percentage of QC-rejected WVCs in the second dataset is similar to those presented in table 2-4. The simple combination of SE and MLE filters twice as many WVCs as the MLE-based method, while the MUDH algorithm filters three times more data. In contrast with the VRMS scores of the QC-ed WVCs in table 2-4, the filtered WVCs with the new approaches have a higher VRMS score (see the upper row in each wind speed category) than those filtered by the MLE-based method, indicating that the algorithms proposed in Section 5.2 are very effective in filtering spatially variable winds over all of the wind speed regions.

Table 5. VRMS difference between ASCAT and buoy winds for three different quality control methods.

Wind speed (m/s)	VRMS of rejected WVCs (m/s)			VRMS of kept WVCs (m/s)			QC-ed ratio (%)		
	MLE	SE/MLE	MUDH	MLE	SE/MLE	MUDH	MLE	SE/MLE	MUDH
$4 \leqslant v < 7$	4.07	4.12	4.18	1.53	1.52	1.51	0.31	0.66	1.12
$7 \leqslant v < 10$	5.08	5.28	5.28	1.53	1.52	1.51	0.37	0.68	1.08
$v \geqslant 10$	7.32	7.81	7.68	1.98	1.95	1.94	0.24	0.56	0.81
$v \geqslant 4$	5.04	5.28	5.21	1.63	1.62	1.61	0.32	0.65	1.04

The verification of the MUDH algorithm on the 3000 ASCAT-buoy-ECMWF collocations with rain information is presented in table 6. The conclusion is the same as per table 4, i.e., the filtered rain-free ASCAT winds compare worse to buoys than the non-filtered rain-contaminated winds. It proves that the MUDH algorithm is effective in detecting WVCs with enhanced variability in both rainy and rain-free conditions.

Table 6. The VRMS difference between ASCAT and buoy winds for QC-accepted and rejected data using the MUDH algorithm under different rain conditions.

Wind speed (m/s)	Rain free		Rainy	
	VRMS-Kept	VRMS-Rejected	VRMS-Kept	VRMS-Rejected
$v \geq 4$	1.48	3.11	2.58	5.58

5.3.2 Validation with 25-km-equivalent buoy winds

The ten-minute (10-min) buoy wind point measurement is not representative of the scatterometer 25-km area-mean measurement in case of large sub-WVC wind variability, which usually corresponds to quality-controlled ASCAT retrieved winds. However, buoy wind time series can be used to estimate 25-km equivalent WVC winds. That is, 10-min continuous buoy wind series are averaged to 25-km-equivalent scale and used as reference in the validation. The mean wind direction is computed as follows:

$$\bar{\varphi} = \arctan\left(\frac{-\bar{u}}{-\bar{v}}\right) \tag{8}$$

where the mean wind components are calculated using the following equations,

$$\begin{aligned} \bar{u} &= \frac{1}{M}\sum_{i=1}^{M} -w_i \cdot \sin(\varphi_i) \\ \bar{v} &= \frac{1}{M}\sum_{i=1}^{M} -w_i \cdot \cos(\varphi_i) \end{aligned} \tag{9}$$

where M is the number of 10-min buoy measurements, which is determined by expanding the 10-min-equivalent distance vector in the adjacent time bins (centered on the ASCAT measurement time), until the length of the distance vector reaches the WVC size. The minimum value M is set to be 5 (i.e., buoy time series averages within ±20 min of the ASCAT measurement time). w_i and φ_i represent the wind speed and direction of the i^{th} measurement respectively. The mean wind speed can be derived using either Eq. (10) or Eq. (11),

$$\bar{w} = \sqrt{\bar{u}^2 + \bar{v}^2} \tag{10}$$

$$\bar{w} = \frac{1}{M}\sum_{i=1}^{M} w_i \tag{11}$$

In the presence of large sub-WVC wind variability conditions, the mean wind speed estimated by Eq. (10) is usually lower than that estimated by Eq. (11). The latter is more representative of the scatterometer measurements since it well correlates with the integrated sea surface roughness within the WVC. For example, highly variable winds, i.e., blowing at very different and opposed wind directions, lead to very low mean wind speed according to Eq. (10) (average of the wind components) and relatively higher mean wind speed according to Eq. (11) (average of the wind speeds). The scatterometer receives energy from the different sea-surface wind/roughness contributors within the WVC and, as such, well correlates with Eq. (11). In this paper, the mean buoy wind speed is therefore calculated using Eq. (11).

In Table 7, the mean standard deviations of the continuous buoy wind components are presented for the operational QC-ed WVCs, SE/MLE QC-ed WVCs, MUDH QC-ed WVCs, and for WVCs with |MLE|<0.5 and SE>0. It shows that the proposed QC methods are filtering WVCs with similar high sub-WVC wind variability than those filtered by the MLE-based QC. As expected, the filtered WVCs by the different QC approaches have much higher local wind variability than those with |MLE|<0.5 and SE>0 (last row), further confirming that combining MLE and SE results in a good sub-WVC variability indicator.

Table-7: The mean SD values of the continuous buoy wind components for different categories

	SD (speed, m/s)	SD (direction, °)	SD (u, m/s)	SD (v, m/s)
MLE	1.24	27.7	1.66	1.62
SE/MLE	1.27	32.1	1.62	1.61
MUDH	1.29	34.9	1.60	1.73
|MLE|<0.5, SE>0	0.37	6.3	0.47	0.52

Table 8 presents the same VRMS scores as the last row of Table 5 but using the 25-km-equivalent buoy winds instead of the 10-min buoy winds as reference. The VRMS scores are smaller in Table 8 than in Table 5 (last row) indicating that the 25-km-equivalent buoy winds are indeed more representative of ASCAT winds than the 10-min buoy wind point measurements, notably in high sub-WVC wind variability conditions (i.e., the rejected WVCs). In [20], Vogelzang et al estimated the quality of ASCAT and 10-min buoy winds on the scatterometer scale and found that the buoy error variance contribution to the vector difference variance is 72 % while the ASCAT 12.5-km contribution is only 28% for the accepted WVCs, i.e., scatterometer winds are in general of much higher quality than buoy point-measurement winds at scatterometer scales. The time averaging presented here reduces the variance of the ASCAT and buoy vector difference around 38% and 29% for both accepted and rejected WVCs, respectively. Following [20], this would imply that the time-averaged buoy error and the ASCAT 12.5-km contribution would be resp. 55% and 45% for accepted WVCs, i.e., scatterometer winds are in general of similar quality to that of time-averaged buoy winds at scatterometer scales. Temporally averaged buoy winds thus do clearly better represent 25-km spatially-averaged winds. Since the time averaging reduces both the rejected and accepted WVC variances in similar amounts, the wind variances appear rather scalable and wind errors appear mainly due to enhanced wind variability rather than rain contamination and other effects associated with convection, for the rejected cases. In other words, the VRMS scores are dominated by representativeness errors, which explains the large VRMS differences between accepted and rejected WVCs. As such, all wind measurements (ASCAT, buoys and ECMWF) are expected to be of lower quality for rejected cases than the equivalent qualities for accepted WVCs.

Table-8: VRMS difference between ASCAT and 25-km-equivalent buoy winds for three different quality control methods

Wind speed (m/s)	VRMS of rejected WVCs (m/s)			VRMS of kept WVCs (m/s)		
$v \geq 4$	MLE	SE/MLE	MUDH	MLE	SE/MLE	MUDH
	4.14	4.34	4.39	1.29	1.28	1.27

The quality of the rejected WVCs category however is not the same for the three wind data sources. In particular, ECMWF winds are shown in [10] to be of very poor quality under high wind variability conditions. The already discussed VRMS reduction after buoy temporal averaging suggests that indeed buoy errors increase with wind variability since a one-dimensional or 1-D (temporal) averaging becomes less representative of a true 2-D WVC-mean wind (i.e., ideally measurable by spatially averaging a set of buoys evenly distributed over a 25-km WVC) as the sub-cell wind variability increases. However, to conclude on the actual contribution of both ASCAT and buoy wind errors to the high VRMS scores shown in Table 8 (rejected category), further analysis is required, e.g., triple collocation [20].

5.3.3 Test case

Figure 11(*a*) shows an ASCAT wind field with TMI RR values superimposed. The operational QC rejects some WVCs under heavy rain (see the gray arrows around 6.0°N and 177.5°E), but those appear quite consistent spatially. Many other WVCs with more or less rain are not rejected, but those are more erratic. As presented in [10], a more constrained MLE threshold may not be effective in filtering the wind artifacts. For example, at the position denoted by a triangle (where TMI RR=8.9 mm/h), the ASCAT wind inversion residual is relatively low (MLE=-5.5) and the retrieved wind speed and direction are 5.51 m/s and 15.3° respectively. While the collocated buoy measurement shows a wind speed = 3.4 m/s, and wind direction= 280° (the temporally averaged buoy wind and direction are 4.1 m/s and 265.5° respectively), indicating that the ASCAT-retrieved wind is not representative of the buoy wind over there. Fig. 11(*b*) illustrates the time series of 10-min buoy winds (see the solid line with triangle markers) as compared to the ASCAT measurement (see the square marker, first-rank/selected solution; and the circle marker, second-rank solution) for this particular ASCAT-buoy collocation.

Fig. 12(*a*) and (*b*) illustrate the rejected winds (gray arrows) using the QC methods that are presented in Section 5.2.1 and 5.2.2, respectively. It is clear that the new methods reject more WVCs than the operational QC in rainy regions and their vicinity, in line with the increased wind variability denoted by SE. The MUDH algorithm indeed filters more WVCs than the SE/MLE (e.g., the areas around 2.9°N and 177.5°E, 6.2°N and 180°E). The WVC at the position denoted by a triangle, which corresponds to high wind variability, is also filtered by the MUDH technique.

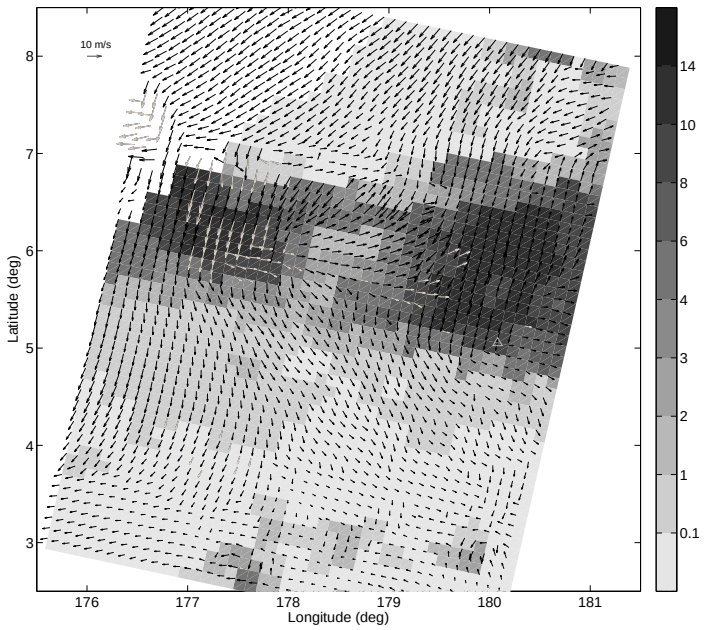

(*a*)

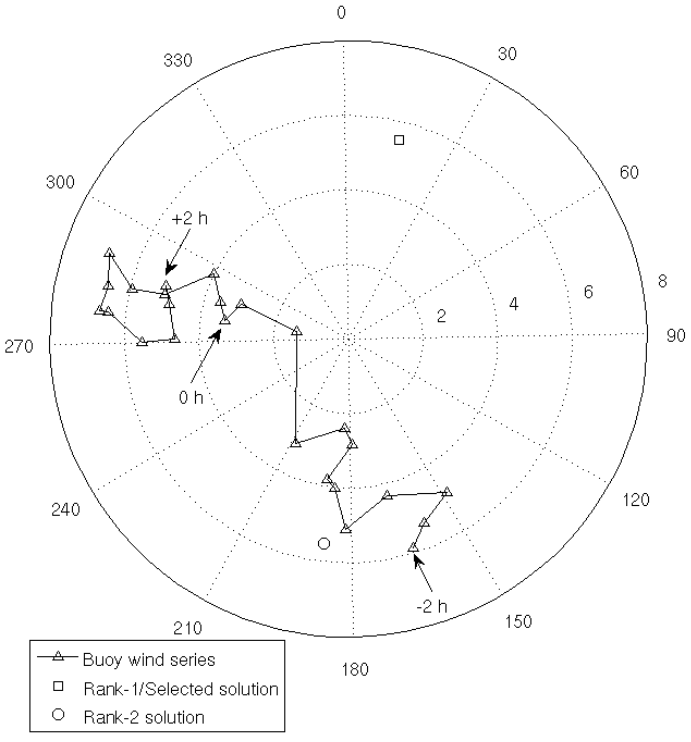

(*b*)

Fig. 11. (a) ASCAT wind observed on December 15, 2009, at 21:17 UTC, with collocated TMI RR superimposed (see the legend). The black arrows correspond to QC-accepted WVCs, and the gray ones correspond to QC-rejected WVCs. The buoy measurements (denoted by the triangle) were acquired at 21:20±2 hours UTC, as shown in the polar coordinate plot (b). The square marker indicates the ASCAT first-rank solution, which is also the selected solution; the circle marker shows the ASCAT second-rank solution.

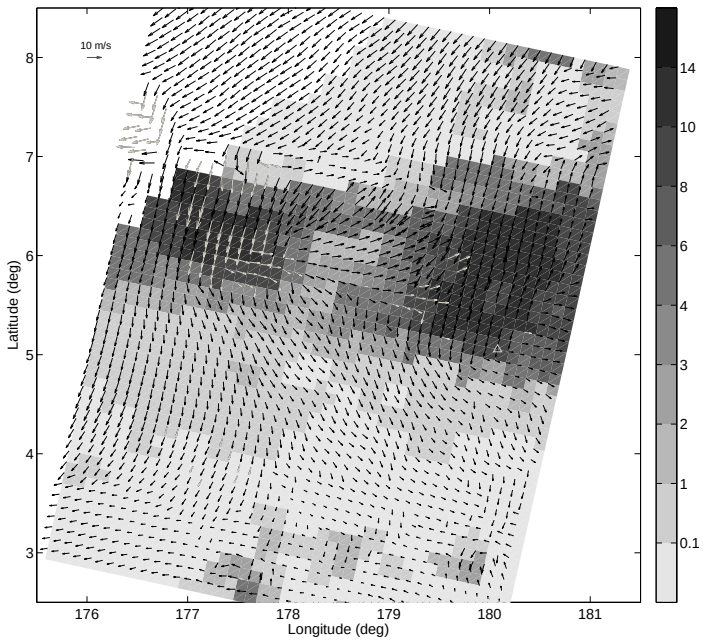

(*a*)

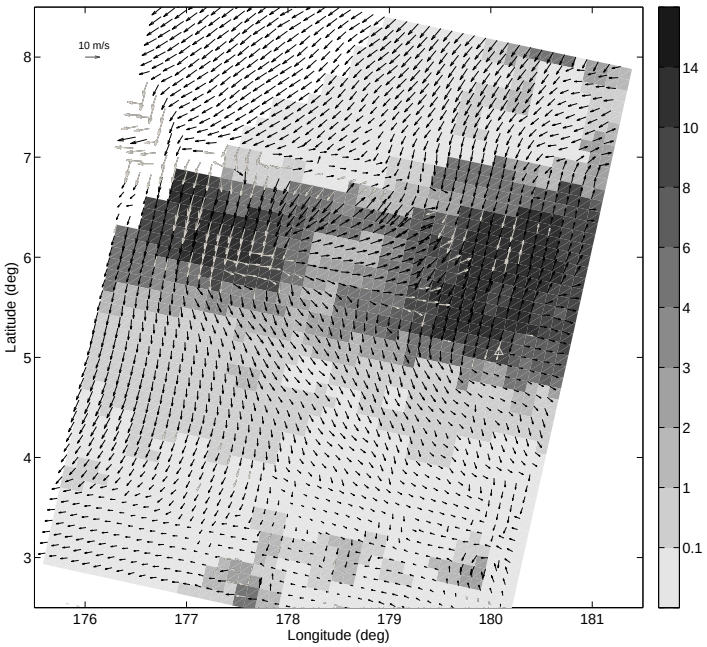

(*b*)

Fig. 12. Illustration of the rejected WVCs (gray arrows) using (a) the combined SE/MLE analysis and (b) the MUDH technique. The gray ones correspond to QC-rejected WVCs. The buoy measurements (denoted by the triangle) were acquired at 21:00 UTC.

6 Conclusions

In this study, a new image processing technique, the so-called singularity analysis, is adapted for ASCAT for the detection of geophysical effects associated with rain and tested for QC purposes. It is shown that SA successfully exploits the rain information content (rain signatures) present in the different ASCAT parameters, and thus an effective rain-contamination detection tool emerges. Moreover, SA detects some rain-impacted WVCs when the MLE-based QC does not, and vice versa, indicating that both techniques have complementary properties.

The correlation between the ASCAT wind quality and a few ASCAT-derived parameters, i.e., MLE, K_p and SE, is also investigated. The three parameters are indeed well correlated with sub-WVC wind variability. MLE detects increased sub-WVC wind variability notably at low and medium wind speeds while SE and K_p detect it at a wider wind speed range. According to the assessment of the MLE-based QC under rainy conditions [10], there is a substantial number of WVCs with low MLE value in heavy rain with poor validation, which needs further evaluation. In order to improve the filtering of ASCAT poor-quality winds, two new algorithms are proposed, which combine MLE with other quality-sensitive parameters.

The SE is proven to be a complementary parameter to MLE for ASCAT QC purposes, particularly in finding large sub-WVC variability cases under rainy conditions. The combination of SE and MLE is first investigated to improve the QC. This method can be refined by taking the K_p and wind speed parameters into account, leading to the development of the MUDH algorithm. The multi-parameter-based QC approaches are developed using ECMWF wind reference and validated using buoy wind reference. The 10-min buoy validation results show that the proposed SE/MLE and MUDH methods filter, respectively, twice and three times as many WVCs as the current MLE-based QC for ASCAT wind speeds above 4 m/s. In particular, more data are filtered by the new methods near convection (rain). The filtered WVCs compare as well to buoys as those screened by the operational MLE-based method.

However, spatial and temporal representativeness are dominating the quality indices, therefore posing a challenge in verification of the QC scheme, i.e., are local buoys or the ECMWF model representative of the scatterometer area-mean vector wind? In particular, where rain is spatially erratic, it induces downbursts of wind on the ocean surface with strong gust fronts and as such rain is associated with enhanced wind variability. Wind verification of a QC scheme by buoy data thus may be penalizing conditions with such high wind variability, since the wind vector measured at a buoy location is generally expected to differ much from the scatterometer wind in case of high wind gradients. A method to convert 10-min buoy wind data to 25-km equivalent winds is proposed and used for QC verification. Temporally-averaged buoy winds do clearly better represent 25-km spatially-averaged winds. Since the time averaging reduces both the rejected and accepted variances in similar relative amounts, wind variances appear scalable and wind errors appear mainly due to enhanced wind variability for the rejected cases, i.e., representativeness errors dominate the VRMS differences between ASCAT and buoy winds. Therefore, all wind measures (ASCAT, buoys and ECMWF) are expected to be of lower quality than the equivalent qualities in kept WVCs. While it is clear that, at scatterometer scales, ECMWF wind errors are high and buoy errors considerably increase under large sub-cell wind variability, ASCAT errors remain unassessed. The proposed

methods are effective in detecting variable winds over all the wind speed and RR regimes. Variable winds are a potential hazard in some applications, such as data assimilation and the methods developed here may be useful for those applications. For other applications, such as nowcasting and oceanography, it may be relevant to keep the flagged WVCs since they provide essential information on (highly variable) air-sea interaction processes that cannot be captured by any other wind observing system.

As already mentioned, the ASCAT wind quality seems to be mainly associated with large sub-WVC wind variability. Further work to quantify independent ASCAT, buoy, and ECMWF wind errors (e.g., triple collocation analysis) needs to be carried out. Also, no evidences of a rain splashing signature and/or and other effects associated with convection (e.g., sea state) have been found in this study. Future work will focus in determining whether these effects do significantly contribute to ASCAT wind quality degradation or not, notably at low winds.

SeaWinds rain studies at Ku-band [1][2][4][6] have all used buoy and NWP model comparison for detecting rain contamination. Although rain effects will be much more prominent in SeaWinds, the effects of wind variability elaborated in this manuscript, will certainly contribute to the trade-off exercise that led in these studies to the QC scheme implementation. Therefore, SeaWinds QC needs to be revisited too in the light of the findings described in this report.

Further analysis is required when applying the proposed method on ASCAT products. Although the edge effects of singularity analysis have been reduced by the description in section 3.1, its performance has not yet been examined specifically. Furthermore, future work will also focus on analysing the correlation between singularity fronts and ASCAT backscatter measurements in particular, since they have not yet been adopted by the singularity analysis. For such purpose, ASCAT Level 1B Full Resolution backscatter data will be exploited, since at smaller footprints the rain splashing signal (among other non-wind signals), being patchy and intermittent, is expected to become more evident.

SA uses the information present in the ASCAT data itself and, as such, is useful for both ASCAT near-real-time products and offline products. The SA code has been optimized for near-real-time processing.

Note that this report is based on references [16] and [21].

Acknowledgments

The work has been funded under the EUMETSAT Ocean and Sea Ice (OSI) Satellite Application Facility (SAF) Associated Scientist project (reference OSI_AVS_12_04). The ASCAT level 1b data are provided by EUMETSAT. The software used in this work has been developed through the EUMETSAT Numerical Weather Prediction SAF. The ECMWF data are retrieved from the ECMWF MARS archive. The TMI data are available from the web site of Remote Sensing Systems (http://www.ssmi.com/). We thank Jean-Raymond Bidlot and ECMWF for providing the GTS buoy wind dataset (already quality controlled). The buoy rain data and buoy wind time series have been obtained from http://www.pmel.noaa.gov/.

Acronyms and abbreviations

Name	Description
AMI	Active Microwave Instrument
ASCAT	Advanced scatterometer
AWDP	ASCAT Wind Data Processor
BUFR	Binary Universal Form for Representation (of meteorological data)
CMOD	C-band geophysical model function used for ERS and ASCAT
CSIC	Consejo Superior de Investigaciones Científicas
ECMWF	European Centre for Medium-Range Weather Forecasts
ERS	European Remote sensing Satellite
ESA	European Space Agency
EUMETSAT	European Organization for the Exploitation of Meteorological Satellites
GMF	Geophysical Model Function
GTS	Global Telecommunication System
KNMI	Koninklijk Nederlands Meteorologisch Instituut (Royal Netherlands Meteorological Institute)
METOP	Meteorological Operational satellite
MLE	Maximum likelihood estimator
NWP	Numerical Weather Prediction
OSI	Ocean and Sea Ice
QC	Quality Control
RR	Rain rate
SA	Singularity Analysis
SAF	Satellite Application Facility
SD	Standard Deviation
SE	Singularity Exponent
TMI	Tropical Rainfall Measuring Mission's (TRMM) Microwave Imager
WVC	Wind Vector Cell

References

[1] J. N. Huddleston and B. W. Stiles, "A multi-dimensional histogram technique for flagging rain contamination on QuikSCAT", in *Proc.IEEE Int. Geosci. Remote Sens. Symp.*, Honolulu, HI, 2000, vol. 3,pp. 1232–1234.

[2] M. Portabella and A. Stoffelen, "A comparison of KNMI quality control and JPL rain flag for SeaWinds", *Can. J. Remote Sens.*, vol. 28, no. 3, pp. 424–430, 2002.

[3] B. W. Stiles and S. H. Yueh, "Impact of rain on spaceborne Ku-band windscatterometer data", *IEEE Trans. Geosci. Remote Sens.*, vol. 40, no. 9,pp. 1973–1983, Sep. 2002.

[4] K. A. Hilburn, F. J. Wentz, D. K. Smith, and P. D. Ashcroft, "Correcting active scatterometer data for the effects of rain using passive microwave data", *J. Appl. Meteorol. Climatol.*, vol. 45, no. 3, pp. 382–398,Mar. 2006.

[5] D. W. Draper and D. G. Long, "Simultaneous wind and rain retrieval using SeaWinds data", *IEEE Trans. Geosci. Remote Sens.*, vol. 42, no. 7,pp. 1411–1423, Jul. 2004.

[6] C. Nie and D. G. Long, "A C-band scatterometer simultaneous wind/rain retrieval method", *IEEE Trans. Geosci. Remote Sens.*, vol. 46, no. 11,pp. 3618–3632, Nov. 2008.

[7] D. E. Weissman, M. A. Bourassa, J. J. O' Brien, J. S. Tongue, "Calibrating the QuikSCAT/SeaWindsRadar for Measuring Rain rate Over the Oceans", *IEEE Trans Geosc and Rem. Sens.*, vol. 41, No.12, pp.2814-2820, Dec. 2003

[8] V. G. Torsekar, "Oceanic rain identification using multi-fractal analysis of QuikSCAT sigma-0", *Master Thesis*, University of Central Florida, Orlando, 2005.

[9] M. Portabella, A. Stoffelen, A. Verhoef, and J. Verspeek, "A new method for improving scatterometer wind quality control", *IEEE Trans. Geosci. Remote. Sens. Lett.*, 9, 579–583, 2012.

[10] M. Portabella, A. Stoffelen, W. Lin, A. Turiel, A. Verhoef, J. Verspeek, and J. Ballabrera, "Rain effects on ASCAT wind retrieval: Towards an improved quality control", *IEEE Trans. Geosci. Remote. Sens.*, vol. 50, no. 7, pp.2495-2506, 2012.

[11] O. Pont, A. Turiel, and C.J. Perez-Vicente, "Empirical evidences of a common multifractal signature in economic, biological and physical systems", *Physica A*, 388:2025–2035, 2009.

[12] O. Pont, A. Turiel, and H. Yahia, "An optimized algorithm for the evaluation of local singularity exponents in digital signals", in: Aggarwal, J., Barneva, R., Brimkov,V., Koroutchev, K., Korutcheva, E. (eds.) *14th International Workshop, IWCIA2011. Lecture Notes in Computer Science (LNCS)*, vol. 6636, pp. 346–357. Springer, Madrid, Spain (2011). Available: http://hal.inria.fr/inria-00581057/en/

[13] C. Anderson, H. Bonekamp, C. Duff, J. Figa-Saldaña, and J.J.W. Wilson, " Analysis of ASCAT ocean backscatter measurement noise", *IEEE Trans. Geosci. Remote. Sens.*, vol. 50, no. 7, pp.2449-2457, 2012.

[14] A. Turiel, M. Portabella, W. Lin, and J. Ballabrera-Poy, "Quality assessment of ASCAT wind vector maps through singularity analysis", *SMOS BEC Technical Note*, BEC-TN.2012.02 v.1, Feb. 2012. [Online] Available: www.smos-bec.icm.csic.es/publications

[15] A. Stoffelen, and D. Anderson, "Scatterometer data interpretation: measurement space and inversion,"*J. Atmos. Ocean. Technol.*, 14(6), 1298–1313, 1997.

[16] W. Lin, M. Portabella, A. Stoffelen, A. Turiel, and A. Verhoef, "Rain identification in ASCAT winds using singularity analysis," *IEEE Trans. Geosci. Remote. Sens. Lett.,* vol 11, no 9, pp. 1519-1523, 2014.

[17] A. Stoffelen and D. Anderson, "Ambiguity removal and assimilation of scatterometer data," *Q.J.R. Meteorol. Soc.*, 123, pp. 491–518, 1997. doi: 10.1002/qj.49712353812.

[18] A. Verhoef, M. Portabella, A. Stoffelen, and H. Hersbach, "CMOD5.n- the CMOD5 GMF for neutral winds," *Ocean and Sea Ice SAF Technical Note*, SAF/OSI/CDOP/KNMI/TEC/TN/165 v.1, May 2008. Available from http://www.knmi.nl/scatterometer/publications/

[19] M. Portabella, and A. Stoffelen, "Characterization of residual information for SeaWinds quality control," *IEEE Trans. Geosci. Remote Sens.*, vol. 40, no. 12, pp.2747–2759, 2002.

[20] J. Vogelzang, A. Stoffelen, A. Verhoef, and J. Figa-Saldaña, "On the quality of high-resolution scatterometer winds," *J. Geophys. Res.,* 116, C10033, doi:10.1029/2010JC006640, 2011.

[21] W. Lin, M. Portabella, A. Stoffelen, A. Verhoef, A. Turiel, "Singularity analysis: a complementary technique for ASCAT wind quality control", *IEEE Trans. Geosci. Remote. Sens.*, submitted in April 2014.